Current Research in Food Science 12 (2026) 101327

Contents lists available at ScienceDirect

Current Research in Food Science

journal homepage: www.sciencedirect.com/journal/current-research-in-food-science

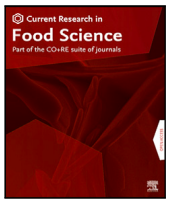

Research paper

FEM modeling of hamburger pan cooking: Fat content influence and neural network-based prediction of fat loss

E. Hernández-Alhambra [a], P. Guiu [b], A. Ferrer-Mairal [b], M.A. Martínez [a,c], B. Calvo [a,c], J. Grasa [a,c,*], M.L. Salvador [b]

[a] Aragón Institute of Engineering Research (i3A), Universidad de Zaragoza, Spain
[b] Instituto Agroalimentario de Aragon IA2, Universidad de Zaragoza-CITA, Miguel Servet 177, 50013 Zaragoza, Spain
[c] Centro de Investigación Biomédica en Red en Bioingeniería, Biomateriales y Nanomedicina (CIBER-BBN), Spain

ARTICLE INFO

Handling editor essor Alejandro G.Marangoni

Keywords:
Pan cooking
Computational model
Beef meat
Fat content
Hamburger
Time flipping
Tenderness
Juiciness

ABSTRACT

In this study, we developed an improved contact-cooking model that incorporates variations in fat content and its retention capacity, aiming to accurately simulate products with different compositions. The proposed approach incorporates the structural heterogeneity of meat by distinguishing between muscle fibers and interstitial fluid, and simulates the transport of water and fat between these regions. The model also accounts for heat transfer and meat deformation, representing the tissue as a hyperelastic material. The computational framework was implemented for the pan-cooking of hamburgers with different fat contents (ranging from 3% to 24%) and periodic flipping during the process. To validate the model, cooking experiments were performed. Although increasing fat content did not significantly affect water loss or core temperature ($p > 0.05$), it strongly influenced other critical aspects of cooking performance and product quality, such as surface temperature, fat loss, total cooking losses, and shrinkage. These changes are relevant because they impact texture and consumer perception. In addition, hamburgers with a higher fat content exhibited lower hardness, cohesiveness, gumminess, and chewiness. The model successfully predicted these trends, demonstrating its potential to capture fat-related effects beyond thermal behavior and enabling the use of model-generated data for the training, validation, and testing of a simple neural network to predict fat loss during the cooking of hamburgers with varying water, fat, and protein contents.

1. Introduction

During pan cooking, meat undergoes structural alterations that result in water and fat losses, shrinkage, and consequent changes in the firmness and juiciness of the final product. As temperature rises, muscle proteins denature and contract, diminishing water-holding capacity and promoting water loss by evaporation and dripping (Szpicer et al., 2022; Mathijssen et al., 2023). Fat melts and migrates toward the surface, contributing to dripping losses (Shilton et al., 2002). Consequently, the coupled movement of water and fat within the meat strongly influences heat transfer and weight loss.

Fat content plays a central role in these transformations. Higher intramuscular fat enhances tenderness and juiciness by increasing lubrication and stimulating salivation during consumption (Duconseille et al., 2022; Vu et al., 2022; Zhang et al., 2024; Shi et al., 2025), while also modulating the thermal and physical behavior of the meat matrix. High-fat meat tends to heat more rapidly at the surface, favoring browning and crust formation and potentially elevating the formation of undesirable compounds (Onopiuk et al., 2021). In contrast, lean meat maintains a surface temperature closer to 100 °C for longer due to greater surface water availability (Shilton et al., 2002). Moreover, reduced average spacing between fat particles at higher fat levels promote the formation of continuous channels that facilitate fat migration and alter heat- and mass-transfer patterns (Oroszvári et al., 2006a; Tornberg, 2013). Therefore, the interaction between fat content and water holding capacity is pivotal in determining the overall texture, juiciness, and weight loss of the cooked meat Tornberg (2013), Duconseille et al. (2022), Zhang et al. (2024).

Numerical modeling of meat contact-heating has emerged as a valuable tool to understand the transformations occurring in meat during thermal processing, enabling the identification of the factors that govern the attainment of a target degree of doneness that ensures microbiological safety while preserving tenderness and juiciness. By coupling heat and mass transfer mechanisms, several models have successfully correlated cooking conditions with temperature distribution (Pan et al.,

* Corresponding author at: Aragón Institute of Engineering Research (i3A), Universidad de Zaragoza, Spain.
E-mail address: jgrasa@unizar.es (J. Grasa).

https://doi.org/10.1016/j.crfs.2026.101327
Received 21 July 2025; Received in revised form 15 January 2026; Accepted 25 January 2026
Available online 27 January 2026

2000; Zorrilla and Singh, 2003) or water loss (Oroszvári et al., 2006a; Moya et al., 2021b; Hernández-Alhambra et al., 2024); established optimal flipping conditions (Moya et al., 2021a; Dalvi-Isfahan, 2023; Hernández-Alhambra et al., 2025); or defined the parameters necessary to achieve microbial safety (Ou and Mittal, 2007; de Albuquerque et al., 2019; Sheen et al., 2024).

Many models describe water transport induced by the contraction of the protein matrix using the Flory–Rehner theory of swelling or shrinking polymer gels, incorporating water transport through Darcy's law (van der Sman, 2007; Ahmad et al., 2015; Chapwanya and Misra, 2015; Nelson et al., 2020). Some models explicitly consider matrix shrinkage as the deformation of a hyperelastic porous medium (Zorrilla and Singh, 2003; Dhall and Datta, 2011; Moya et al., 2021b; Hernández-Alhambra et al., 2024, 2025). However, with few exceptions (Dhall et al., 2012; Dalvi-Isfahan, 2023), most of these models neglect fat transport, because it represents a smaller fraction compared to water and is difficult to model due to its discontinuous phase and complex migration mechanisms, thereby limiting the analysis of fat's impact on transformations during cooking.

The accurate simulation of the cooking process of meat products with varying compositions presents a significant challenge for existing mathematical models. This study addresses this issue through the following objectives: (i) to develop a generalized model that reflects the physiological structure of meat as a porous, multiphase medium composed of a solid matrix and interstitial fluids. The model will couple water and fat transport with heat transfer, account for the deformation of the meat as a hyperelastic material, and incorporate the effect of product flipping during contact cooking on a hot surface; (ii) to assess the contribution of fat content to cooking losses and heat transport, validating the obtained findings with experimental data; (iii) to predict fat loss during the cooking of meat with different compositions using a feedforward neural network.

To achieve these objectives, the applicability of the model proposed by Dhall et al. (2012) will be extended by incorporating meat shrinkage due to cooking losses and protein matrix contraction. Additionally, the model will be implemented for the pan-cooking of hamburgers, considering the flipping process during cooking. Hamburgers can contain up to 30% fat; therefore, neglecting fat transport in these products may lead to inaccurate predictions. Nevertheless, the homogeneity in the initial fat distribution alleviates, to some extent, the complexity of the phenomena involved. Computational results will be validated against experimental data obtained using a domestic induction hob, where monitoring the evolution of temperature, moisture loss, and fat loss, product shrinkage, and textural parameters of the hamburgers will be assessed.

2. Materials and methods

2.1. Hamburger preparation

Patties were prepared from the central portion of the loin (*Longissimus dorsi muscle*) of Blonde d'Aquitaine and Angus veal. Lean and adipose tissues were separated by trimming from muscle to remove visible subcutaneous and intermuscular fat. Each fraction was ground using a 3-mm grinder plate. Formulations were prepared by weight and mixed to ensure a homogeneous distribution of fat particles, with fat contents of 3%, 14%, and 24% (w/w), denoted A3, A14, and A24 for Angus and B3 for Blonde d'Aquitaine. These fat levels were selected to span the commercial range for hamburgers ranging from 3% to 27% fat (Brewer, 2012). The blends were moulded into cylindrical patties (100 mm diameter, around 20 mm thickness, and 180 g weight) using a manual hamburger press. Each hamburger was individually stored at 4 °C in LDPE zip-seal bags for 12–14 h, being equilibrated to 20 °C in an isothermal chamber (MIR-153 Incubator, Sanyo, Osaka, Japan) before cooking.

2.2. Water holding capacity (WHC) and fat holding capacity (FHC)

The WHC was assessed following the methodology described by Hernandez-Alhambra (2024), based on the approach outlined by Goñi and Salvadori (2010). Minced meat patties of approximately 9 g were placed inside open plastic bags and subjected to thermal treatments by immersion in a thermostatic water bath (Digiterm S-150, JP Selecta, Abrera, Spain) at temperatures ranging from 30 °C to 100 °C for 30 min. Immediately after heating, samples were rapidly cooled in an ice-water bath. The final moisture content of the patties, used as an indicator of WHC, was determined by measuring the weight difference before and after drying in a convection oven at 105 °C for 24 h (AOAC International, 2002). The bags retained the exudate released from the meat during heating. To remove water, the bags were dried at 105 °C for 24 h. The residue remaining in the bags after drying was taken as the fat not retained by the meat during thermal treatment. Each temperature and product were tested in ten independent replicates. Results were expressed as kg of water or kg of fat per kg of dry matter.

2.3. Cooking procedure

Each hamburger was individually cooked in a 210 mm diameter multilayer pan (composed of a 0.6 mm steel bottom layer, a 3.6 mm aluminum core, and a 0.8 mm steel top layer) with a Teflon platinum non-stick coating (WMF, WMF Group GmbH, Geislingen an der Steige, Germany). The pan was heated using an induction hob equipped with an automatic temperature control system "frying sensor" (BOSCH PXY675DW4E/01 model, BSH, Munich, Germany). The experimental setup is illustrated in Fig. 1. Cooking was carried out at a set pan temperature of 215 °C. The hamburgers were placed in the pan once a surface K-type RS PRO thermocouple (RS, London, UK) confirmed that a stable temperature (±3 °C from the setpoint) had been reached. To monitor the central bottom temperature of the pan, a K-type thermocouple (1.5 mm in diameter) was inserted into a pre-drilled hole. Each hamburger was cooked for 680 s, with three flips performed at regular time intervals. The induction hob's power adjustments required to maintain the target temperature were recorded using LabTech software v6.0.1.5 (ConnectWise, Tampa, FL, USA). The temperature at the center of the hamburger was measured using a 1.5 mm-diameter T-type penetration thermocouple. All thermocouples were connected to a data logger (TC-08 Series, Farnell Components, Barcelona, Spain). Additionally, product weight was continuously monitored every 5 s with a precision of 0.1 g using a balance (DS30K0.1 L, Kern & Sohn, Balingen-Frommern, Germany), which was placed beneath the induction hob. The average temperature of the upper surface of the samples was assessed using images captured before and after each flip by an infrared thermal camera (Testo 875-2 model, Lenzkirch, Germany). The infrared camera was calibrated by placing crumpled aluminum foil, assumed to act as a near-perfect reflector, in front of the sensor for measurement of the reflected apparent temperature. Prior to cooking measurements, the ambient relative humidity and viewing distance were recorded and set according to manufacturer instructions. For the measurement of meat surface temperature, an emissivity value of 0.95 was applied. Five independent replicates were performed for each experimental condition.

2.4. Cooking loss, moisture loss, fat loss and shrinkage

Cooking loss was defined as the proportion of liquid expelled during the cooking process, which may include water, fat, proteins, and minerals. This value was expressed as a percentage, calculated by comparing the weight of the hamburger before and after cooking, relative to its raw weight. The moisture loss was estimated to correspond to the weight loss obtained through continuous measurements using the balance located beneath the cooking system. Fat loss was calculated using two methods: based on the compositional analysis data of raw

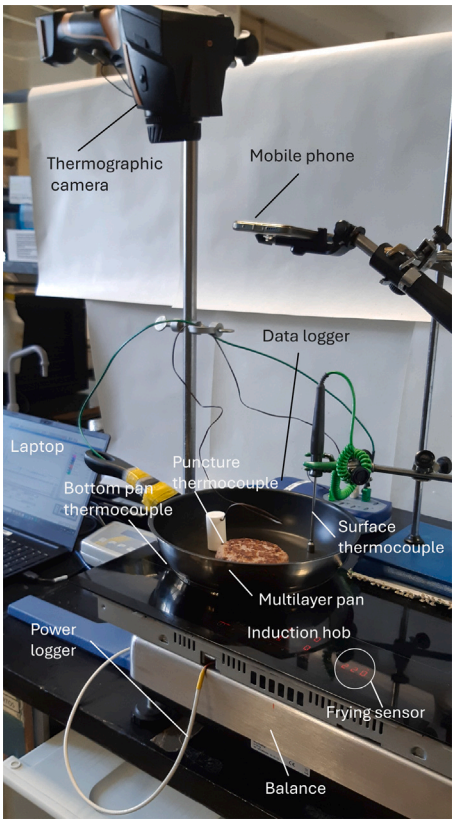

Fig. 1. Experimental setup for temperature and weight loss measurement during the cooking process.

and cooked hamburgers, and through mass balance, considering fat loss as the difference between cooking loss and moisture loss. This assumption involves disregarding protein or other meat component losses, but it is justified as the protein percentage in the pan residue, expressed on a wet basis, did not exceed 2.91% in any case. Both moisture and fat losses were expressed as a percentage based on the weight of the hamburger. The appearance of both raw and cooked hamburgers is presented in Fig. 2, highlighting the shrinkage in size associated with thermal processing. Hamburger shrinkage was assessed by two methods: (a) As the percentage reduction of the surface area of the upper side, determined from digital image analysis using the open-source ImageJ software. Images were captured with a Samsung Galaxy A8 mobile phone equipped with a 16MP camera (resolution 4608 × 3456 pixels) positioned parallel to the pan at 50 cm under diffuse LED lighting (5500 K). (b) As the percentage decrease in the volume of the hamburger after cooking and cooling to achieve a constant weight (30 min). The volume was determined following the method of Yan et al. (2008) based on the Archimedes principle as described in Hernández-Alhambra et al. (2025). These determinations were carried out in quintuplicate.

2.5. SEM

The surface morphology of both raw and cooked hamburgers was analyzed using an environmental scanning electron microscope (ESEM, Quanta FEG 250), which was employed to obtain scanning transmission electron microscopy (STEM) images at 10 kV. For each experimental condition, SEM images were acquired from three different hamburgers.

2.6. Moisture, fat and protein content

Moisture, fat, and protein contents were determined in both raw and cooked hamburgers in triplicate. In cooked hamburgers, moisture content was first determined as an average value across the entire hamburger. However, the distribution of moisture within the hamburger was also assessed. To this end, four cylindrical samples (20 mm in diameter) were taken from each of the three analyzed hamburgers using a cylindrical punch. Each sample was then sectioned into three parts: two outer layers, each 3 mm thick (with the one that made first contact with the pan referred to as the upper layer), and a third section representing the central region. The moisture content was determined by drying the sample in an electrically heated oven at 103 ± 2 °C to constant mass, following the ISO official method 1442 (ISO, 2023). Fat content was determined by Soxhlet extraction using petroleum ether, following prior hot acid hydrolysis with hydrochloric acid. The procedure was carried out in accordance with official method 1443 (ISO, 1973). Protein content was determined by elemental nitrogen analysis using the Dumas combustion method, following the procedures described in ISO official method 16634-1 (ISO, 2008). The nitrogen content obtained was converted to crude protein using a nitrogen-to-protein conversion factor of 6.25, as recommended for beef.

2.7. Malondialdehyde (MDA) analysis

Quantification of lipid peroxidation products through the TBARS (thiobarbituric acid reactive substances) assay was performed by measuring malondialdehyde equivalents, following a method adapted from (Sobral et al., 2020). Briefly, 10 g of meat were homogenized with 20 mL of 10% (w/v) trichloroacetic acid (TCA) using an Ultra-Turrax homogenizer (Jake and Kunkel, Staufen, Germany) at 20 000 rpm for 90 s. This step facilitates the release of MDA from the tissue matrix and simultaneously precipitates proteins. The homogenate was then centrifuged at $3\,000 \times g$ for 5 min at 4 °C, and the resulting supernatant was filtered through qualitative filter paper. A second TCA precipitation was performed to further remove protein residues. After centrifugation under the same conditions, the new supernatant was collected and pooled with the previous one. An aliquot of 2 mL of the combined extract was mixed with 2 mL of a 20 mM thiobarbituric acid (TBA) solution prepared in glacial acetic acid. The mixture was homogenized and incubated in a water bath at 97 °C for 20 min to promote the formation of the MDA-TBA complex. After cooling to room temperature, the absorbance of the resulting chromogen was measured at 532 nm using a UV/VIS spectrophotometer (Unicam 5625, Cambridge, UK). MDA concentration was determined from a calibration curve constructed with 1,1,3,3-tetramethoxypropane in the range of 0.164–1.625 mg/L. Results were expressed as mg MDA/kg of sample.

2.8. Texture

The textural properties of the hamburgers were assessed using a TA-XT2i Plus Texture Analyzer (Stable Micro Systems, Godalming, UK) equipped with a 30 kg load cell. Texture Profile Analysis (TPA) was conducted on cuboidal samples measuring $25 \times 25 \times 20$ mm, which were obtained from the hamburgers after equilibrating to room temperature. A double compression test was applied using a 50 mm diameter cylindrical flat-probe, acting at a speed of 1 mm s^{-1} up to 50% deformation and triggered at a force of 0.049 N. Twenty replicates were evaluated for each condition. The instrument automatically recorded force (N) versus time (s) curves, from which the following parameters were derived: hardness (the peak force during the first compression cycle), springiness (the ratio of the distance recovered during the second compression to that of the first), cohesiveness (the ratio of the area under the second compression curve to that of the first), and chewiness (calculated as the product of hardness, cohesiveness, and springiness). In addition, shear force measurements were performed using a Warner-Bratzler blade, operated at 1 mm s^{-1} up to a penetration depth of 35 mm, with the same trigger force. From the resulting force-time graph, the initial peak force (corresponding to the onset of penetration), the maximum shear force, and the total work of shearing (area under the curve) were determined.

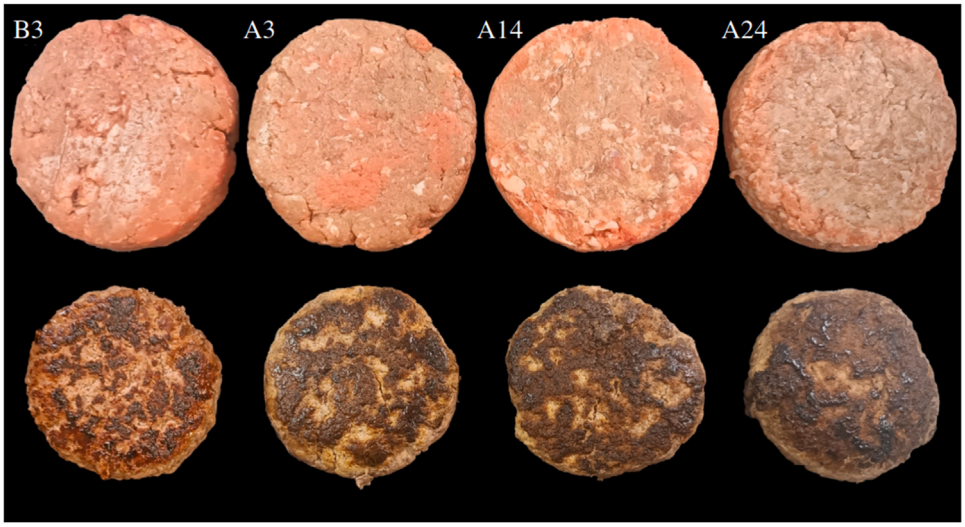

Fig. 2. Raw product (upper zone) and cooked product (lower zone).

2.9. Neural network for predicting fat loss

A feedforward neural network was developed to predict fat loss in hamburgers based on their composition. The model takes three input features corresponding to the initial mass fractions of fat and water ($X_{f,0}$ and $X_{w,0}$), while the initial protein mass fraction was obtained as $X_{p,0} = 1 - X_{w,0} - X_{f,0}$. The analysis focuses exclusively on these three components because fat, water, and protein constitute the major constituents of meat products and play a dominant role in determining their physicochemical behavior during cooking. Other minor components, such as ash, carbohydrates, and trace compounds, were not included in the FEM model since their proportions in hamburger formulations are typically low.

The appropriate neural network architecture will be determined through iterative experimentation, balancing complexity and performance (further specific details of the neural network are described in Section 6). In this case, the network is trained using data generated from the cooking simulations, which provide detailed insights into fat loss based on initial composition. Validation techniques and hyperparameter tuning help refine the architecture to ensure good generalization without overfitting.

2.10. Statistical analysis

To assess whether variations in fat content and cattle breed influenced the measured parameters, a one-way analysis of variance (ANOVA) was applied. Post-hoc comparisons were performed using Tukey's Honestly Significant Difference (HSD) test to identify statistically significant differences among groups. The null hypothesis stated that neither fat level nor breed had a significant effect on the results. Statistical analyses were conducted using the Statistical Package for the Social Sciences, version 26 (SPSS Inc., Chicago, IL, USA). A $p < 0.05$ was considered indicative of statistical significance.

3. Mathematical model

To mathematically describe the problem, meat is modeled as a porous medium composed of a solid matrix and pore space. The solid matrix consists of protein, bound fat, and bound water (p, sf, and sw), while the pore space contains two fluid components: liquid water and liquid fat (w and f). During thermal processing, mass transfer may occur between these five phases, such as the release of bound water into the pore space or the incorporation of liquid fat into the solid matrix. These transfers are referred to as phase change fluxes within the model, describing the exchange of mass between the defined meat constituents. The solid matrix represents the muscle fibers, consistent with physiological descriptions of meat (Tornberg, 2005), and the pore space corresponds to the interstitial fluid. The phase change fluxes considered in the model (between bound and free water, and between bound and free fat) are illustrated in Fig. 3 by the arrows indicating the direction of mass exchange between phases.

In raw meat, most water and fat are retained within the solid matrix: water inside myofibrils and fat near connective tissue. As temperature rises, fat melts but remains largely trapped within the matrix. Continued heating induces protein denaturation and contraction of the connective tissue network, releasing water that migrates beyond the matrix. Liquefied fat is also released; however, due to its lower content compared to water, fat behaves as a dispersed phase and only migrates when sufficient channels form upon melting (Dhall et al., 2012). During cooking, meat is assumed to remain fully saturated with liquid (Dhall and Datta, 2011). Food materials in the rubbery state are treated as deformable porous media whose pores remain filled with liquid phases (water and fat). Under these conditions, no gas phase exists within the structure, and evaporation occurs only at the surface. This assumption provides a physically sound basis for coupling heat and mass transfer and accurately represents moisture and fat migration within the meat matrix.

Mechanical comminution markedly modifies the structural organization of meat (Berger et al., 2023), resulting in hamburger patties where muscle fibers and fiber bundles remain largely intact but are randomly dispersed. This contrasts with the highly organized, anisotropic architecture of whole-muscle tissue (Tornberg, 2005). Consequently, this randomized structure is considered an appropriate representation for modeling hamburger systems and can therefore be treated as an isotropic material.

The fundamental equations governing the model are outlined below and are organized into the following subsections.

3.1. Mass transfer

The mass conservation equations proposed by Dhall et al. (2012), along with those describing evaporation rates and mass transfer between intra- and extracellular regions, are summarized in Table 1 for the different phases (fat, bound fat, water, bound water, and protein). In Table 1 the concentration of each phase is defined as $c_i = \phi_i \rho_i$, where $i = p, f, sf, w, sw$. Here, $\dot{m}_w$ and $\dot{m}_f$ denote the mass transfer rates from solid matrix water and fat to the pore space. Although hamburger patties are assumed to remain fully saturated with liquid

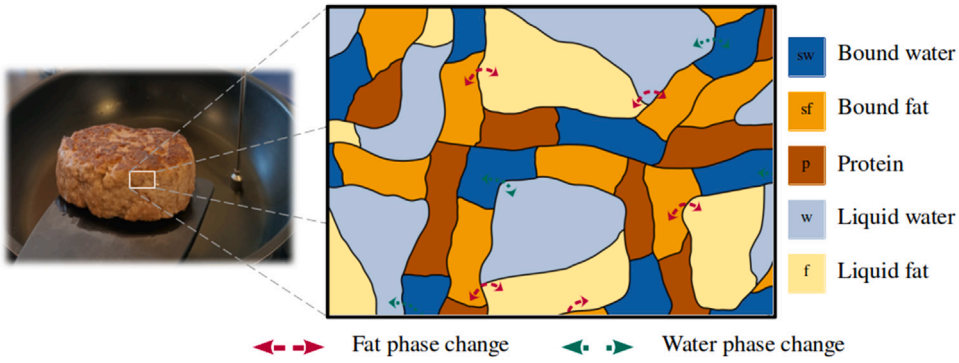

Fig. 3. Meat structure and phase change fluxes present in this problem. The different phases present in the problem, water and liquid fat (inside the pore, w and f) as well as protein, bound water and bound fat (in the solid matrix, p, sw and sf) are included and represented with light and dark colors, respectively.

Table 1
Mass transfer equations for all the phases included in the model.

Phase	Mass conservation equations	Sources and fluxes	
Liquid water	$\frac{\partial}{\partial t}(c_w) + \nabla \cdot \mathbf{n}_{w,G} = -\dot{I}_w + \dot{m}_w$	Evaporation Water from solid	$\dot{I}_w = \dot{I} - \dot{I}_{sw}$ $\dot{m}_w = K_1(c_{sw} - c_{sw,eq})$
Liquid fat	$\frac{\partial}{\partial t}(c_f) + \nabla \cdot \mathbf{n}_{f,G} = \dot{m}_f$	Fat from solid	$\dot{m}_f = K_2(c_{sf} - c_{sf,eq})$
Bound water	$\frac{\partial}{\partial t}(c_{sw}) + \nabla \cdot \mathbf{n}_{sw,G} = -\dot{I}_{sw} - \dot{m}_w$	Evaporation	$\dot{I}_{sw} = \frac{c_{sw}}{c_w + c_{sw}}\dot{I}$
Bound fat	$\frac{\partial}{\partial t}(c_{sf}) + \nabla \cdot \mathbf{n}_{sf,G} = -\dot{m}_f$		
Protein	$\frac{\partial}{\partial t}(c_{pr}) = 0$		

during cooking, and therefore no evaporation occurs, the equations are presented in their most general form by including the terms $\dot{I}_w$ and $\dot{I}_{sw}$, which represent the evaporation rates from pore space water and bound water, respectively. These terms, describing evaporation within the bulk, can be expressed as:

$$\dot{I} = \dot{I}_w + \dot{I}_{sw} = \Gamma_w \left(\rho_{v,eq}^{(w)} - \rho_v\right) + \Gamma_{sw}(\rho_{v,eq}^{(sw)} - \rho_v) \tag{1}$$

Both rates are modeled as a non-equilibrium relaxation toward the local equilibrium vapor density, with distinct kinetic coefficients Γ_w and Γ_{sw} to capture the different evaporation dynamics of free and bound water. The determination of these functions is non-trivial, as their forms and parameters depend on local thermodynamic fields such as temperature and water activity, interfacial area, and microstructural features, all of which are difficult to measure and calibrate. Specifically, $\rho_{v,eq}^{(w)}$ denotes the equilibrium vapor density for pore water, whereas $\rho_{v,eq}^{(sw)}$ corresponds to the equilibrium vapor density for bound water. The local vapor density ρ_v appears in both terms, ensuring that evaporation occurs only when the vapor phase is undersaturated relative to the local equilibrium state.

The normal flux for each liquid phase ($i = w, f$) is defined as:

$$\mathbf{n}_{i,G} = \mathbf{n}_{i,s} + c_i \mathbf{v}_{s,G} \tag{2}$$

where $\mathbf{v}_{s,G}$ is the solid velocity and $\boldsymbol{n}_{i,s}$ corresponds to the absolute flux of liquid water and fat that can be defined by the diffusivity due to concentration gradients, D_i, and due to the thermal gradients $D_{i,T}$:

$$\mathbf{n}_{i,s} = -\nabla(D_i c_i) - \nabla(D_{i,T} T) = -\nabla(D_i c_i) - \nabla\left(D_i \frac{\partial c_{i,eq}}{\partial T} T\right) \tag{3}$$

3.2. Heat transfer

It is assumed that there is no internal heat generation in the food; heat transfer arises solely from pan heating and water phase-change effects. The latent heat of fat melting is neglected, as it is much smaller than that of water evaporation–typically by a factor of 15–25, depending on fat composition. The initial temperature and composition are uniform throughout the hamburger. Thus, the heat transfer process can be modeled using the following energy balance for the multicomponent system:

$$\rho_{eff} c_{p,eff} \frac{\partial T}{\partial t} + \sum \mathbf{n}_{i,G} c_{p,i} \nabla T = \nabla \cdot (k_{eff} \nabla T) - L_{evap}(\dot{I}_{sw} + \dot{I}_w) \quad (i = w, f) \tag{4}$$

where $\rho_{eff}, c_{p,eff}, k_{eff}$ are the thermal properties as a function of temperature and composition that were calculated considering the three components (protein, fat, and water) that compose the food (Hernández-Alhambra et al., 2024).

3.3. Solid mechanics.

To formulate the mathematical model, the volume fraction ϕ_i for each phase must be defined as follows:

$$\phi_i = \lim_{V \to 0} \frac{V_i}{V}, \qquad V = \sum V_i, \qquad \sum \phi_i = 1, \qquad i = p, f, sf, w, sw \tag{5}$$

The kinematics of meat deformation are modeled using a framework commonly employed in the analysis of solids undergoing finite strains (Hernández-Alhambra et al., 2024). To capture the distinct physical processes involved, a series of fictitious intermediate configurations are introduced, leading to a multiplicative decomposition of the deformation gradient $\boldsymbol{F}$. Assuming that the temperature-induced deformation of the is negligible, $\boldsymbol{F}$ can be expressed as the product of three components: the deformation due to water volume loss ($\boldsymbol{F}_M$), protein shrinkage ($\boldsymbol{F}_p$), and the elastic deformation of the solid phase ($\boldsymbol{F}_e$):

$$\boldsymbol{F} = \boldsymbol{F}_M \boldsymbol{F}_p \boldsymbol{F}_e \tag{6}$$

The volume change due to moisture loss, J_M, can be calculated by relating it to the change in the volume fraction, $\phi_M = \phi_w + \phi_f$, of the fluid phases: water and fat.

$$J_M = \frac{1 - \phi_{M,0}}{1 - \phi_M} \tag{7}$$

The moisture deformation gradient is defined by:

$$\boldsymbol{F}_M = J_M^{1/3}\boldsymbol{I} \tag{8}$$

with $\boldsymbol{I}$ the $[3 \times 3]$ identity matrix and the Jacobian raised to the power of $1/3$ to make $\det(\boldsymbol{F}_M) = J_M$.

$$\boldsymbol{F}_p = \begin{bmatrix} \lambda(T) & 0 & 0 \\ 0 & \lambda(T) & 0 \\ 0 & 0 & \lambda(T) \end{bmatrix} \tag{9}$$

This is not true in the general case in Eq. (6) where $\lambda(T)$ is a shortening stretch that takes into account the protein shrinkage dependence on the temperature and is proposed to be:

$$\lambda(T) = \begin{cases} 1 & T \leq 30\ ^\circ\mathrm{C} \\ (\lambda_s - 1)(0.02T - 0.6) + 1 & 30\ ^\circ\mathrm{C} < T < 80\ ^\circ\mathrm{C} \\ \lambda_s & T \geq 80\ ^\circ\mathrm{C} \end{cases} \tag{10}$$

Where λ_s is a parameter representing the maximum protein shrinkage. This temperature-dependent shrinkage parameter was obtained by fitting experimental shrinkage data to the proposed function, while initial estimates were taken from (Hernández-Alhambra et al., 2025).

When neglecting body forces and inertia effects, conservation of linear momentum results in the quasi-static equilibrium equation $\nabla\boldsymbol{\sigma} = 0$ for the material, with $\boldsymbol{\sigma}$ being the total Cauchy stress. Conservation of angular momentum yields the symmetry of this stress tensor, which can be expressed as the sum of the partial solid stress and the partial fluid stress:

$$\boldsymbol{\sigma} = \hat{\boldsymbol{\sigma}}_s + \hat{\boldsymbol{\sigma}}_M \tag{11}$$

where

$$\hat{\boldsymbol{\sigma}}_s = \phi_s\boldsymbol{\sigma}_e \qquad \text{and} \qquad \hat{\boldsymbol{\sigma}}_M = \phi_M\boldsymbol{\sigma}_M = -\phi_M p_M \boldsymbol{I} \tag{12}$$

Here, $\boldsymbol{\sigma}_e$ represents the Cauchy elastic stress of the meat and p_M the volume-averaged pressure exerted by the moisture.

The constitutive law selected for simulating the elastic behavior of the meat is based on the isotropic compressible Neo-Hookean material. The decoupled form of the strain energy function is:

$$\Psi\left(\boldsymbol{C}_e\right) = \Psi_{vol}(J_e) + \bar{\Psi}(\bar{\boldsymbol{C}}_e) = \frac{K}{2}\left(J_e - 1\right)^2 + \frac{G'}{2}\left(\bar{I}_1 - 3\right) \tag{13}$$

where K and G' are the bulk and the shear elastic modulus, $J_e = \det(\boldsymbol{F}_e)$, and $\bar{I}_1 = \mathrm{tr}(\bar{\boldsymbol{C}}_e)$ is the first invariant of the modified (deviatoric) right Cauchy–Green tensor $\bar{\boldsymbol{C}}_e = \bar{\boldsymbol{F}}_e^T\bar{\boldsymbol{F}}_e$, with $\bar{\boldsymbol{F}}_e = J_e^{-1/3}\boldsymbol{F}_e$.

The second Piola–Kirchhoff stress tensor is obtained as the derivative of the strain energy in a non-dissipative process:

$$\boldsymbol{S}_e = 2\frac{\partial\Psi(\boldsymbol{C}_e)}{\partial\boldsymbol{C}_e} = \boldsymbol{S}_{e,vol} + \bar{\boldsymbol{S}}_e = J_e p\boldsymbol{C}_e^{-1} + J_e^{-\frac{2}{3}}(\mathbb{I} - \frac{1}{3}\boldsymbol{C}_e^{-1}\otimes\boldsymbol{C}_e) : \tilde{\boldsymbol{S}}_e \tag{14}$$

where $\boldsymbol{S}_{e,vol}$ and $\bar{\boldsymbol{S}}_e$ are the volumetric and deviatoric parts of the second Piola–Kirchhoff stress tensor, p is the hydrostatic pressure, and $\tilde{\boldsymbol{S}}_e$ is the fictitious second Piola–Kirchhoff stress tensor:

$$p = \frac{d\Psi_{vol}(J_e)}{dJ_e} \qquad \tilde{\boldsymbol{S}}_e = 2\frac{\partial\bar{\Psi}(\bar{\boldsymbol{C}}_e)}{\partial\bar{\boldsymbol{C}}_e} \tag{15}$$

Once the second Piola–Kirchhoff stress tensor $\boldsymbol{S}_e$ is known, the Cauchy stress tensor $\boldsymbol{\sigma}$ can be obtained the push-forward relation $\boldsymbol{\sigma}_e = \frac{1}{J_e}\boldsymbol{F}_e\boldsymbol{S}_e\boldsymbol{F}_e^T$.

4. Finite element model

To simulate the cooking process of a hamburger, a 2D axisymmetric model incorporating the fundamental equations described in the previous section was developed and implemented in COMSOL Multiphysics 6.1.

The geometry of both the pan (210 mm in diameter and 5 mm thick) and the product (100 mm in diameter and 20 mm thick) was considered. The different domains were meshed with rectangular elements using quadratic approximation for mass transfer, heat tranfer, and deformation. A mesh sensitivity analysis was performed to determine the optimal mesh size, which showed stabilization of the solution. The number of nodes and elements in the selected mesh model was 399 and 320, respectively, of which 152 are boundary elements (see Fig. 4, mesh box).

To replicate the process of flipping the hamburger, two pans were modeled following the approach of Hernández-Alhambra et al. (2025), in which the effect of gravity on water diffusion is neglected. Additionally, regarding solid mechanics, deformation along the thickness of the hamburger is considered negligible, allowing the assumption that the hamburger remains confined between the two pan surfaces. The influence of the lower and upper pan domains, illustrated in Fig. 4, on the cooking process is controlled by multiplying the corresponding boundary conditions by a specific function. The two step functions depicted in Fig. 4 determine the moment at which the food is actually flipped and were smoothed to avoid numerical singularities (Hernández-Alhambra et al., 2025).

4.1. Initial and boundary conditions

An initial uniform temperature of 24.5 °C was assigned to both the pan and the hamburger, consistent with experimental conditions. Water and fat initially reside in the solid matrix because of the microstructural characteristics of ground meat: water is largely held within myofibrils and fat clusters remain bound near connective tissue (Tornberg, 2005) and were set to their maximum values satisfying the measured mass fractions ($X_{w,0}$ and $X_{f,0}$). As cooking progresses and temperature rises, these components migrate into the pore space and eventually exit the domain (see Fig. 5).

To replicate the experimental procedure, a power control was incorporated into the model to regulate the heat power required to raise the temperature of the pan (Hernández-Alhambra et al., 2024). Furthermore, the cooking process begins once the pan has reached the target temperature of 215 °C, as in the experiment. The first 175 s were used to heat the pan to the desired temperature. Henceforth, computational results will be presented, excluding this initial heating period.

It is considered important to emphasize that the boundary conditions are the same for each side of the hamburger but are activated and deactivated at complementary cooking times. Thus, when *side 1* is cooked, the boundary conditions marked in dashed boxes in Fig. 4 apply; on the other hand, when *side 2* is cooked, the boundary conditions marked in dotted boxes in Fig. 4 apply.

5. Results and discussion

5.1. Effect of heating on product properties

5.1.1. Water holding capacity and fat holding capacity

The fitted equations for water holding capacity (WHC) and fat holding capacity (FHC) are fourth-order polynomial models that include interaction terms among the variables: temperature (x-axis) and initial fat fraction (y-axis) in the product composition. The inclusion of higher-order terms in the model is motivated by the need to capture nonlinear relationships and interaction effects that arise from the complex physical processes involved. It is important to note that Eq. (16) represents an empirical polynomial fitting to the experimental data, used solely to describe the observed nonlinear behavior within the studied range. The function is not used for prediction or extrapolation purposes, and it is not coupled to the computational model. The coefficients were obtained by least-squares fitting, ensuring smoothness and stability of the surface.

The estimated coefficients of each polynomial term for both WHC and FHC are presented in Table 2. Their units are such that satisfied the units of WHC and FHC ($kg_w/kg_{dry\ product}$ and $kg_f/kg_{dry\ product}$). These values were obtained by fitting the model to experimental data, obtaining a coefficient of determination (R^2) between experimental

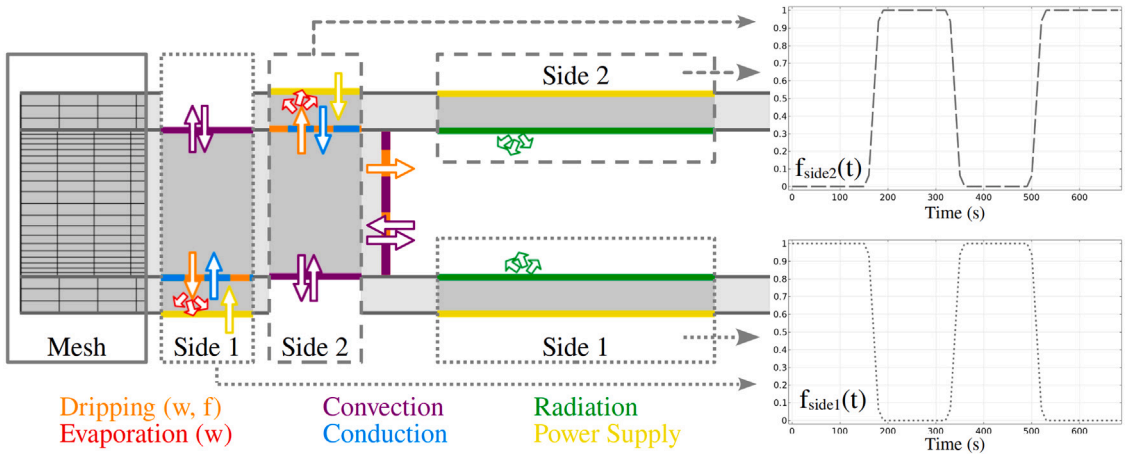

Fig. 4. Finite element model and boundary conditions.

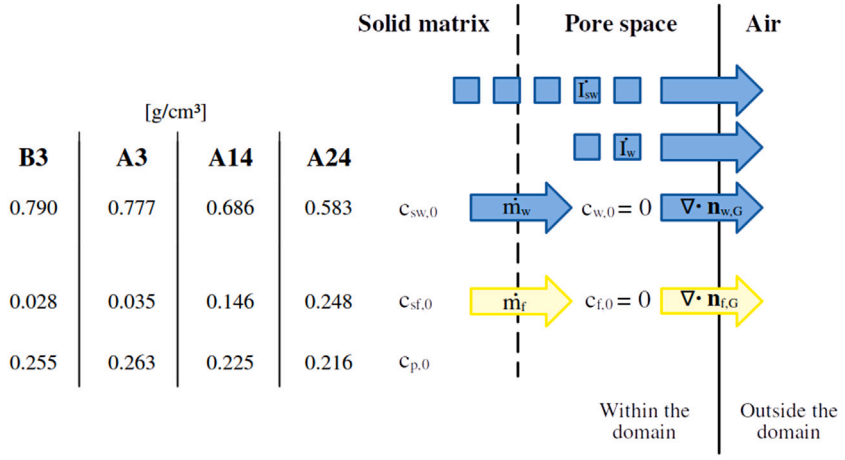

Fig. 5. Schematic representation of the movement of the five phases during the cooking process, along with the initial concentration conditions of all phases in the four products analyzed in this study. Yellow arrows indicate the movement of the fat phase, while blue arrows indicate the movement of the water phase. Water and fat initially reside in the solid matrix due to the starting temperature (24.5 °C).

data and the estimated surface 0.9945 and 0.9925 for WHC and FHC, respectively. Notably, certain coefficients, such as p_{01}, p_{02}, and p_{03}, exhibit relatively large magnitudes, indicating a strong dependence of both WHC and FHC on fat content and its nonlinear contributions. In contrast, coefficients such as p_{40} and p_{31} are small in absolute value, suggesting a limited influence of higher-order temperature effects.

Fig. 6(b) shows the fitted WHC and FHC surfaces across the range of studied temperatures and initial water fractions. These surfaces were incorporated into the model as input data to characterize the full range of possible product compositions.

$$\text{WHC and FHC}(x,y) = p_{00} + p_{10}x + p_{01}y + p_{20}x^2 + p_{11}xy + p_{02}y^2 + p_{30}x^3 + p_{21}x^2y + p_{12}xy^2 + p_{03}y^3 + p_{40}x^4 + p_{31}x^3y + p_{22}x^2y^2 + p_{13}xy^3 \quad (16)$$

5.1.2. Model parameters fitting

The parameters employed in the finite element model (FEM) are summarized in Table 3. Their sources and estimation methods differ, some were obtained directly from experimental measurements, others were extracted from the literature, and a subset was optimized during model calibration to reproduce the observed experimental behavior. Furthermore, several parameters were expressed as empirical functions of the initial fat content ($X_{f,0}$), allowing them to adapt to the composition of each product analyzed. Specifically, two parameters treated as composition based, namely the water and fat diffusivities, are held constant throughout the simulation despite their well-known dependence on the evolution of pore space during the cooking process. This is a limitation of the model and warrants attention in future work, particularly in relation to crust formation.

5.2. Effect of fat content on temperature

Fig. 7(a) shows the experimental temperature evolution at the core of the hamburgers for different fat contents, along with the results obtained from computational simulations. The agreement between simulated and experimental data was generally good, as reflected by the coefficient of determination (R^2) values of 0.7552, 0.7123, 0.9118, and 0.9426, respectively. Additionally, the root mean square error (RMSE) values were 6.77 °C, 7.24 °C, 4.02 °C, and 3.51 °C, respectively, further supporting the accuracy of the simulations, particularly for samples with higher fat content. The final central temperatures measured during the trials were very similar and largely independent of fat content (71.0, 71.8, 72.5, 70.3, and 71.6 °C for B3, A3, A14, and A24, respectively). In agreement, Oroszvári et al. (2006a) reported no significant differences in the temperature profiles of beef hamburgers across fat levels. The potential influence of fat content on core temperature can be rationalized by transport mechanisms and phase changes occurring during pan-cooking. In fat-rich matrices, the convective heat transfer driven by water present in the meat is complemented by fat transport.

Table 2
Model coefficients for WHC ($kg_w/kg_{dry\ product}$) and FHC ($kg_f/kg_{dry product}$) with $i = f, w$. The units of each coefficient are such that the resulting WHC and FHC values are expressed in $kg_i/kg_{dry\ product}$.

Coefficient	Value (WHC)	Value (FHC)	Coefficient	Value (WHC)	Value (FHC)
p_{00}	4.11	0.1173	p_{21}	−0.000631	−0.001342
p_{10}	−0.0008667	0.00159	p_{12}	−7.89	−0.2916
p_{01}	−62.2	−1.879	p_{03}	−1107	−185.1
p_{20}	−0.0007871	$-4.056\cdot10^{-5}$	p_{40}	$1.406\cdot10^{-9}$	$1.536\cdot10^{-10}$
p_{11}	0.953	0.03223	p_{31}	$4.47\cdot10^{-6}$	$1.025\cdot10^{-5}$
p_{02}	468.3	60.55	p_{22}	−0.0006085	−0.001672
p_{30}	$4.661\cdot10^{-6}$	$1.571\cdot10^{-7}$	p_{13}	18.86	1.538

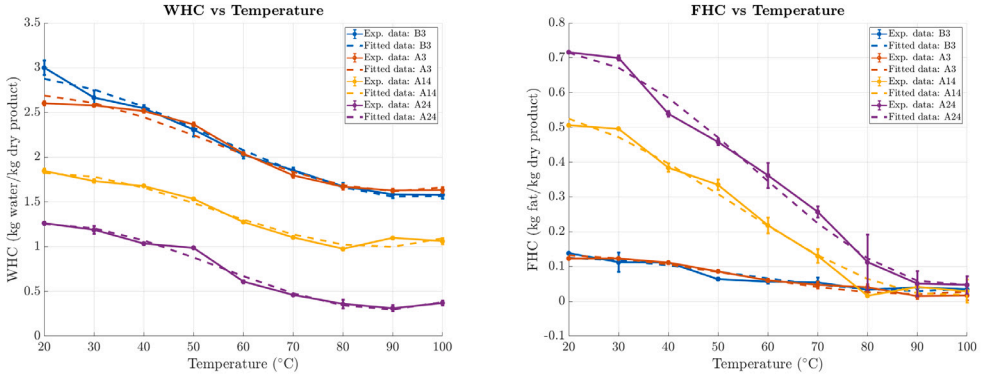

(a)

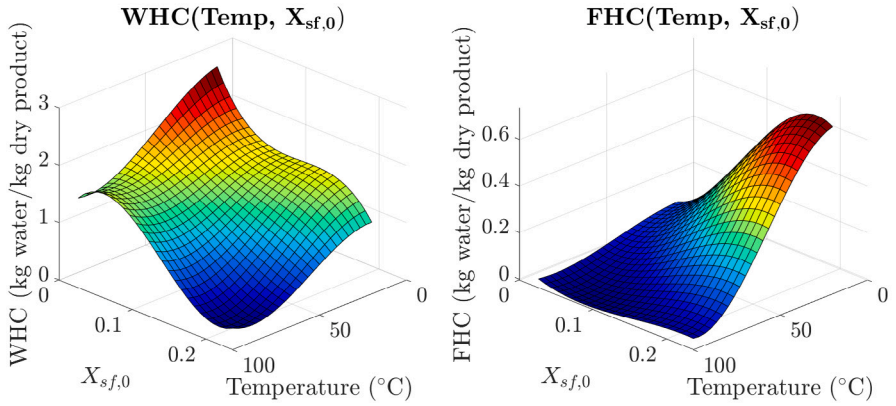

(b)

Fig. 6. (a) Evolution of WHC and FHC, of both fitted (dashed line) and experimental data (continuous line) for every composition analyzed. (b) Polynomial regression for WHC (left) and FHC (right) depending on temperature (T) and the initial fat mass fraction ($X_{f,0}$).

If the fat melting point-which ranges from 32.22 to 47.5 °C depending on the fatty acid composition (Otto et al., 2022) has been exceeded, fat is also released from the solid matrix into the extracellular space and may eventually escape through dripping (Shilton et al., 2002). Notwithstanding this additional convective pathway, the present data indicate no measurable increase in core temperature attributable to fat transport. Consistent with our observations, Pan et al. (2000) showed that the contribution of mass transport to the evolution of core temperature is small when comparing measured center temperatures with model predictions that either include or neglect mass-transfer effects. Moreover, any minor enhancement in local convection is offset by the decrease in bulk thermal conductivity as fat fraction increases. As a result, the net effect of increasing fat content on heat penetration remains negligible at the product core. A further mechanism is the displacement of the interfacial vapor layer by dripping fat, which could increase hamburger-pan contact conductance. However, such an interface effect does not necessarily translate into higher core temperatures. During frying, a boiling (evaporation) region forms beneath the dehydrated surface layer; the associated latent-heat demand imposes a strong cap on inward heat flux and thus limits temperature rise toward the center. The extent of the dehydration zone is difficult to quantify, but it is less than 2 mm, since the temperature recorded 2 mm above the bottom surface approaches 100 °C without exceeding it (Hernández-Alhambra et al., 2024). Immediately after turning the samples, infrared thermography showed maximum surface temperatures of 124.2, 134.0, 154.4, and 158.7 °C were recorded for B3, A3, A14, and A24, respectively. These results indicate that the maximum surface temperature increases with the fat content. During cooking, the surface of the patty in contact with the pan undergoes profound structural changes that result in the formation of a crust. The surface irregularities produced by these changes lead to uneven pan-patty contact, so that the actual contact conductance does not correspond to a single value. This causes large temperature variations across the surface, with differences reaching up to 70.3 °C. Fig. 7(c) shows the evolution of the mean, maximum, and minimum experimental surface temperatures together with the computational predictions. As observed, the mean

Table 3
Model input parameters.

Name and description	Value	Source
Model parameters		
$K_{control}$ controller parameter [W/°C]	84	Fitted
W_{max} Maximum induction hob power [W]	2200	Measured
T_{amb} surrounding air temperature [°C]	24.5	Measured
T^{o}_{pan} pan objective temperature [°C]	215	Measured
P_{amb} environment pressure [kPa]	$1.013 \cdot 10^{2}$	Measured
H_c thermal conductance [W/(m^2 K)]	$31.07X^{2}_{f,0} - 32.21X_{f,0} + 40.88$	Fitted
h convection coefficient [W/(m^2 K)]	5	Fitted
Water properties		
$\overline{\rho}_w$ water density [kg$_i$/m^3]	997.2	Choi and Okos (1986)
D_w water diffusivity [m^2/s]	$4.696 \cdot 10^{-9}X^{2}_{f,0} - 7.668 \cdot 10^{-10}X_{f,0} + 1.784 \cdot 10^{-11}$	Fitted
$C_{p,w}$ water specific heat [kJ/(kg K)]	$4.1289 - 9.0864 \cdot 10^{-5} \cdot T + 5.4731 \cdot 10^{-6} \cdot T^{2}$	Choi and Okos (1986)
k_w water thermal conductivity [W/(m K)]	0.57	Choi and Okos (1986)
L_{evap} vaporization latent heat [J/kg]	$2.26 \cdot 10^{6}$	Straub (1985)
h_m mass transfer coefficient [m/s]	$174X^{3}_{f,0} - 31.79X^{2}_{f,0} + 1.832X_{f,0} - 0.008701$	Fitted
σ_{evap} evaporation ratio [1/s]	$1.0028 \cdot 10^{-3}$	Fitted
K_{evap} surface evaporation constant [1/s]	$169.5X_{f,0} - 1.298$	Fitted
K_{evap} surface evaporation constant [1/s]	$169.5X_{f,0} - 1.298$	Fitted
K_1 constant for mass transfer from solid matrix fat to pore space [1/s]	$0.01662X^{2}_{f,0} - 0.006804X_{f,0} + 0.0006778$	Fitted
K domain evaporation constant [1/s]	0.0001	Fitted
Fat properties		
$\overline{\rho}_f$ fat density [kg$_i$/m^3]	$9.2559 \cdot 10^{2} - 4.1757 \cdot 10^{-1} \cdot T$	Choi and Okos (1986)
D_f fat diffusivity [m^2/s]	$0.0026X^{2}_{f,0} - 0.0004204X_{f,0} + 9.751 \cdot 10^{-6}$	Fitted
$9.2559 \cdot 10^{2} - 4.1757 \cdot 10^{-1} \cdot T$ $C_{p,f}$ fat specific heat [kJ/(kg K)]	$1.9842 + 1.4733 \cdot 10^{-3} \cdot T - 4.8008 \cdot 10^{-6} \cdot T^{2}$	Choi and Okos (1986)
k_f fat thermal conductivity [W/(m K)]	$1.8071 \cdot 10^{-1} - 2.7604 \cdot 10^{-4} \cdot T - 1.7749 \cdot 10^{-7} \cdot T^{2}$	Choi and Okos (1986)
K_2 constant for mass transfer from solid matrix fat to pore space [1/s]	$1.941X^{2}_{f,0} - 0.2751X_{f,0} + 0.006157$	Fitted
Protein properties		
$\overline{\rho}_p$ protein density [kg$_i$/m^3]	1330	Choi and Okos (1986)
$C_{p,s}$ protein specific heat [kJ/(kg K)]	$2.0082 + 1.2089 \cdot 10^{-3} \cdot T - 1.3129 \cdot 10^{-6} \cdot T^{2}$	Choi and Okos (1986)
k_p protein thermal conductivity [W/(m K)]	$1.7881 \cdot 10^{-1} + 1.1958 \cdot (10^{-3}) \cdot T - 2.7178 \cdot (10^{-6}) \cdot T^{2}$	Choi and Okos (1986)
WHC [kg water/kg dry material]	Fig. 6(b) left.	Measured
FHC [kg water/kg dry material]	Fig. 6(b) right.	Measured
G' storage modulus [kPa]	$G'(T)_b = \begin{cases} 0.0007341 \cdot T^3 - 0.07776 \cdot T^2 + 2.335 \cdot T + 3.466 & \text{if } 25\ °C \le T < 55\ °C \\ 42.35 + \frac{25.62}{(1+0.838\exp(0.2492(T-65.91)))} & \text{if } 55\ °C \le T < 80\ °C \\ -0.4494 \cdot T + 77.3 & \text{if } 80\ °C \le T < 100\ °C \end{cases}$	Hernández-Alhambra et al. (2024)
λ_S shrinkage effect parameter	$20.29X^{3}_{f,0} - 8.09X^{2}_{f,0} + 0.4111X_{f,0} + 0.9895$	Fitted

temperature on the top surface of the hamburgers after flipping increases with fat content. The axisymmetric model assumes uniform contact between the patty surface and the pan; therefore, it cannot reproduce the heterogeneous temperature distribution observed experimentally. As a result, significant discrepancies arise between the mean experimental surface temperatures and the computationally predicted values.

In low-fat hamburgers, the temperature at the surface in contact with the pan remains closer to 100 °C for a longer duration than in higher-fat hamburgers, due to the greater amount of water available for evaporation. In the latter, the dehydrated region progresses inward more rapidly, reducing the energy allocated to evaporation in this zone and thereby allowing a greater temperature increase in the layer adjacent to the pan. This relationship between surface temperature and fat content is consistent with the findings reported by Sheridan and Shilton (2002), although in their study, the hamburgers were cooked using far-infrared radiation.

Fig. 8 illustrates the changes in meat microstructure due to cooking, based on SEM imaging. Visually, structural alterations at the hamburger surface are more pronounced in samples with higher fat content, characterized by larger and more interconnected pores. Similar structural changes resulting from crust formation due to spatial temperature variations have been reported by other authors (Tornberg, 2005; Feyissa et al., 2013). Protein denaturation occurs to a greater extent as fat content increases, due to the higher surface temperatures observed in these cases. As a result, meat permeability near the surface is greater in fat-rich samples. This facilitates fat release through dripping, which displaces steam in the gap between the meat and the pan, increasing thermal contact conductance and further elevating surface temperature. Crust formation also reduces surface smoothness. Areas not in direct contact with the pan contribute to surface temperature variability observed in thermographic images, a phenomenon more evident in high-fat samples.

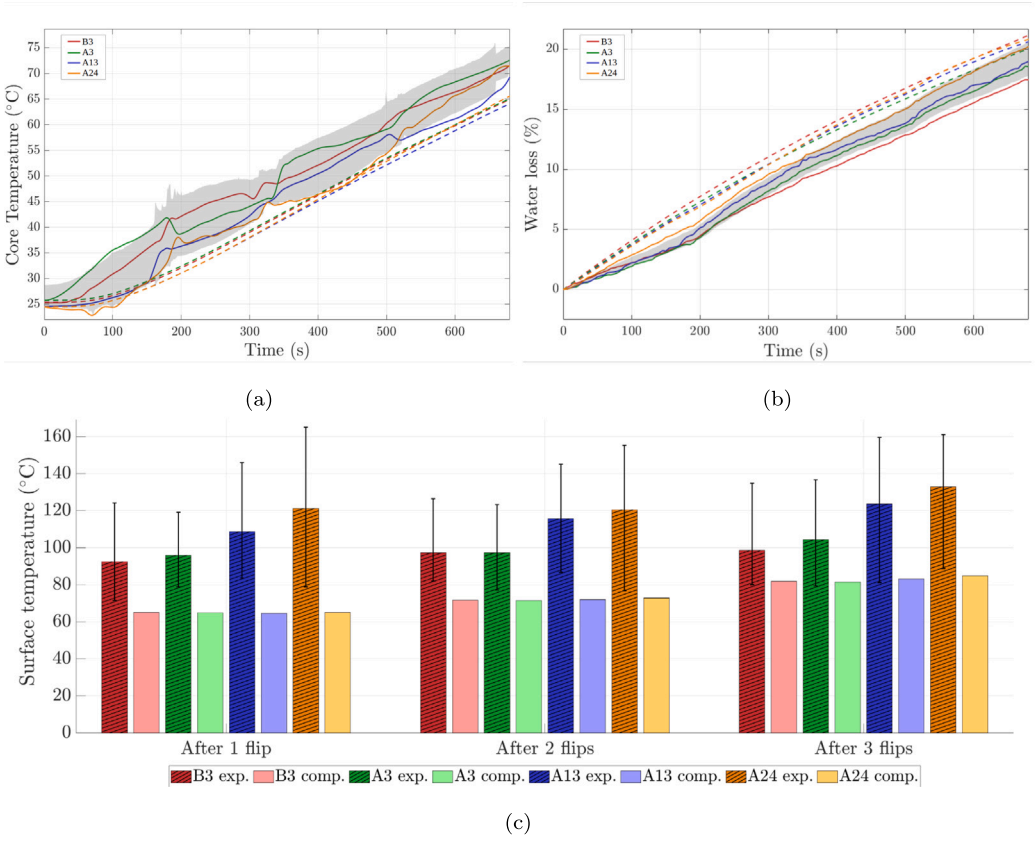

Fig. 7. Comparison between experimental (continuous lines) and simulated (dashed lines). (a) Core temperature and (b) Water loss during pan-frying for four different initial fat mass fractions. Experimental data are shown as mean values, while the shaded areas represent the 99% confidence intervals of the experimental measurements. (c) Comparison between experimental and computational mean surface temperature after each flip for four different initial fat mass fractions. Error bars indicate the range between the coldest and hottest measured points.

Based on these findings, the objective was to verify whether the higher temperatures observed in high-fat hamburgers had an impact on the extent of lipid oxidation reactions during cooking, as it has been reported that lipid oxidation product levels in beef increase with temperature rise (Liu et al., 2023). As a consequence of oxidative spoilage, lipid hydroperoxides are formed, which are unstable and decompose into various secondary products. One of the most important oxidation products is malondialdehyde (MDA), which is often used as a marker of oxidative damage. The obtained results (1.55 ± 0.04 and 1.63 ± 0.06 mg MDA/kg for A3 and A24, respectively) indicated that there were no significant differences ($p > 0.05$) in MDA levels between hamburgers with varying fat content, possibly due to the temperature differences being limited to the most superficial layer. Other authors have also reported no significant differences in TBARS values for beef patties roasted at 150–190 °C, and even a decrease at temperatures above 230 °C (Xia et al., 2021; Liu et al., 2024). This behavior can be attributed to MDA's high reactivity with other meat constituents containing primary amino groups, such as proteins (Roldan et al., 2014).

5.3. Effect of fat content on moisture, fat and cooking losses

Fig. 7(b) shows the evolution of water loss during cooking for the different hamburgers, both experimental and those obtained through numerical simulation. The comparison between simulated and experimental data showed a satisfactory level of agreement. The coefficient of determination (R^2) values, 0.6192, 0.8712, 0.9016, and 0.9694, reflect this consistency across the different samples. In addition, the corresponding root mean square error (RMSE) values of 3.23%, 2.06%, 1.81% and 1.05% further support the reliability of the simulations, particularly in samples with higher fat content where the model performed best.

As observed, moisture loss follows a linear trend over time in all cases. Additionally, as indicated in Table 4, final moisture loss after cooking was not dependent on the fat content of the hamburger ($p > 0.05$), with no significant differences found between breeds for the same fat content. Dhall et al. (2012) also reported that water losses are independent of composition and show a linear relationship with temperature rise. These findings are consistent with those of Oroszvári et al. (2006a), who found no significant influence of the initial water content on water losses during cooking. In this type of cooking, moisture distribution is not homogeneous throughout the product, as shown in Table 4, with a higher moisture content in regions closer to the surface located outside the evaporation front. The losses in these regions are markedly higher in hamburgers with higher fat content, which is consistent with the higher surface temperature of fat-rich samples.

On the other hand, fat losses were greater in samples with higher initial fat content, regardless of the quantification method used (compositional analysis or mass balance), as shown in Table 4. The differences observed between both methods may be attributed to the fact that, when using the mass balance method, disregarding protein losses in samples with lower fat content may result in a higher error margin. The fact that fat losses are higher in samples with a greater initial fat content also influences cooking losses, which are consequently greater. The dependence of fat losses on initial fat content has been reported by other authors with similar findings (Dhall et al., 2012). A plausible explanation for why fat losses increase while moisture losses remain similar as the fat content of hamburgers rises is that the probability

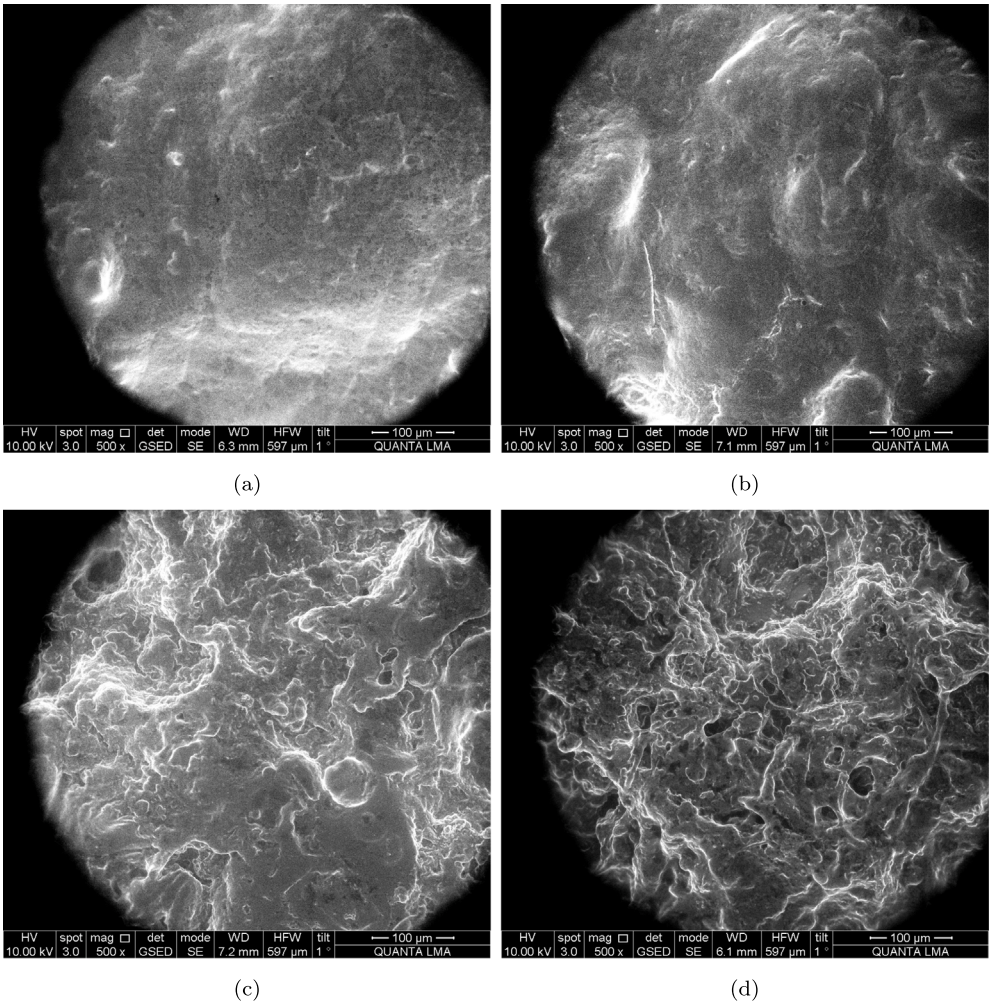

Fig. 8. SEM Images of hamburgers surface. (a) A3 raw. (b) A3 cooked. (c) A24 raw. (d) A24 cooked.

of interactions between fat droplets and adipocytes increases with fat content, given the quadratic dependence between the spacing among fat particles and fat content (Tornberg, 2013). Melted fat accumulates into larger fat clusters and is then transported by pressure-driven contraction toward the surface through fat channels. This mechanism indicates that fat permeability in hamburgers is highly dependent on fat content (Oroszvári et al., 2006a). Moreover, permeability to fat is higher than permeability to water, and the difference becomes greater in fattier meat, reaching up to 100-fold at 50 °C (Oroszvári et al., 2006b), likely due to the fat channels formed during cooking.

Sheridan and Shilton (2002) indicated that, as a consequence of moisture and fat losses during cooking, the fat fraction in fat-rich hamburgers may be lower after cooking than in the raw samples, while in low-fat raw hamburgers, the fat content may increase after cooking. Fig. 9 presents the water, fat, and protein content of the hamburgers before and after cooking, obtained experimentally by compositional analysis and numerical simulation. A good agreement between both methods was observed, with results consistent with those of Sheridan and Shilton (2002), with the following final fat content values: 3.18 ± 0.65%, 4.41 ± 0.82%, 16.40 ± 2.57%, and 22.53 ± 0.58% for B3, A3, A14, and A24, respectively. Assessing fat and moisture losses during cooking is nutritionally relevant, as the initial compositional percentages do not accurately reflect the actual intake. For every 100 g of raw product, the fat consumption will be 2.28 ± 0.51, 3.29 ± 0.65, 11.89 ± 1.58, and 15.45 ± 0.81 g when cooking hamburgers B3, A3, A14, and A24, respectively, which initially contained 2.63 ± 0.84%, 3.33 ± 0.15%, 13.80 ± 2.46%, and 23.70 ± 1.91% fat.

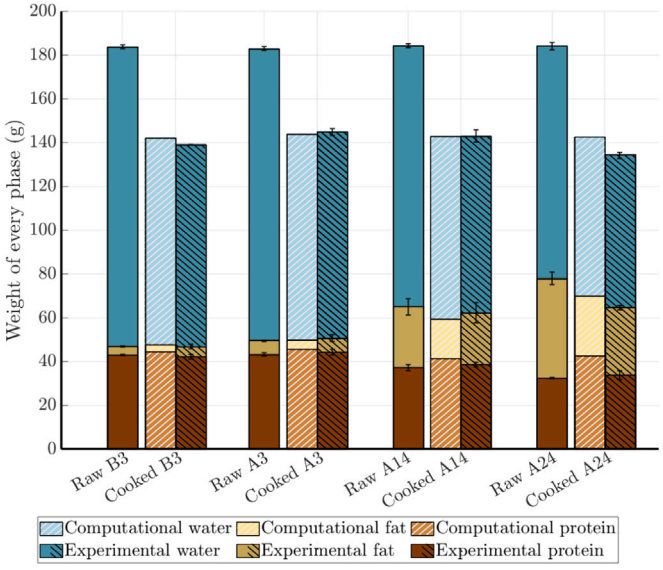

Fig. 9. Water, fat, and protein content in different hamburgers raw (plain colors) and cooked (hatched colors): experimental and simulated data.

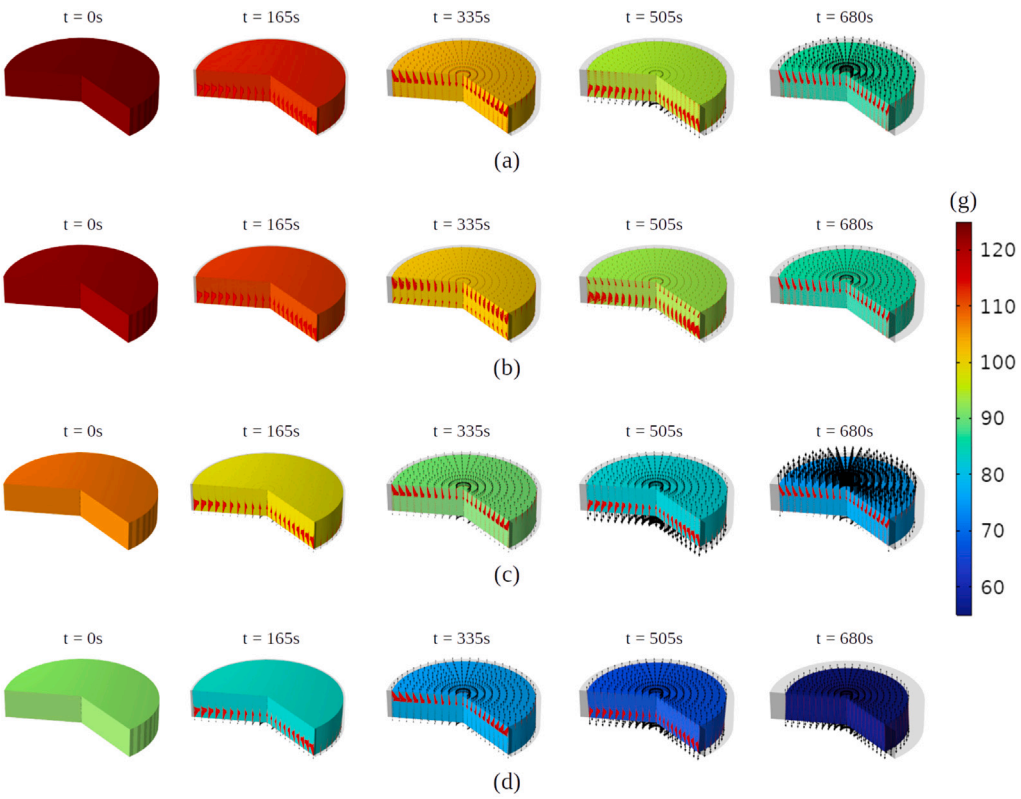

Fig. 10. Amount of water (g) at various time points during cooking for all analyzed hamburgers. Water fluxes (black arrows) and heat fluxes (red arrows) are represented to show their direction. The initial configuration is superimposed with transparency. (a) B3. (b) A3. (c) A14. (d) A24.

5.4. Effect of fat content on shrinkage

During the cooking process, the hamburgers undergo a noticeable reduction in size, which depends on the fat percentage (Fig. 2).This shrinkage is also captured by the model, as shown in Fig. 10, where it is evident how heat fluxes and water loss during cooking contribute to the contraction of the product. Table 4 reflects the change in the surface area of the hamburger evaluated experimentally and numerically. The model predicts that the surface area decreases by 32.13% for a fat content of 24%, compared to a reduction of 23.56% for Angus hamburgers with 3% fat. Shrinkage exhibits higher values than cooking loss, indicating that not all retraction can be attributed solely to liquid losses (Barbera and Tassone, 2006; Dhall and Datta, 2011; Hernández-Alhambra et al., 2024, 2025). However, a strong linear relationship between area shrinkage and cooking loss in ground beef patties has been reported (Niu et al., 2015). Transverse and longitudinal shrinkage of muscle fibers and fiber fragments have been associated with myosin denaturation and actin and/or titin denaturation, respectively (Vaskoska et al., 2021).

Comparing the results obtained with those reported in the literature regarding hamburger shrinkage is challenging since different studies use varying parameters to assess shrinkage: diameter (Zorrilla and Singh, 2003; Oroszvári et al., 2006b), surface area (Hernández-Alhambra et al., 2024; Vu et al., 2022), volume (Vu et al., 2022; Hernández-Alhambra et al., 2025), or thickness (Pan and Singh, 2001; Dhall and Datta, 2011). Additionally, since shrinkage depends on the number of flips (Hernández-Alhambra et al., 2025) and cooking temperature (Hernández-Alhambra et al., 2024), the reported outcomes may vary across studies.

Some studies found no correlation between fat content and shrinkage, as the diameter of patties did not change with the addition of 9% fat to the formulation (Bastos et al., 2014). However, Oroszvári et al. (2006a), in line with the present work, concluded that the diameter of beef patties decreased from 19.6% to 11% when fat content was reduced from 25.9% to 6.1%. Recent studies examining the replacement of animal fat in hamburgers also report a reduction in shrinkage as the proportion of fat substituted by other plant-based components, such as almond flour (Kirkyol and Akköse, 2023) or high internal phase Pickering emulsions (Badar et al., 2024), increases.

5.5. Textural quality

Compressive and cutting yield strains have been demonstrated to be effective mechanical indicators of the textural properties of cooked high-beef-content hamburgers. Among the parameters obtained from texture profile analysis (TPA), hardness and chewiness are particularly suitable for distinguishing between different hamburger formulations (Souppez et al., 2025). Therefore, the texture of the hamburgers was evaluated using both TPA and shear tests, and the results are presented in Table 5. Hardness, cohesiveness, gumminess, and chewiness decreased as the fat content in the patties increased. After cooking, the fat content of samples A14 and A24 was more similar than in their raw state (16.40% and 22.53%, respectively), and thus, no significant differences were observed between these two formulations. However, substantial differences were evident in all measured parameters between A14/A24 and the leaner formulations A3 and B3. Shear tests reflected the same trend, showing lower values for maximum force, first peak force, and work of shearing in samples with higher fat content. These results suggest that tenderness of the hamburger is more closely related to the fat content after cooking than to final moisture content, which was measured at 65.10±0.83%, 64.53±0.81%, 55.93±1.62%, and 51.25±0.78% for B3, A3, A14 and A24, respectively. Juiciness perception has been reported to correlate negatively with cooking loss (Lucherk et al., 2017). On that basis, one might expect higher-fat hamburgers, which often incur greater cooking losses, to be perceived as less juicy. However, multiple studies demonstrate the

Table 4
Moisture, fat and cooking losses and shrinkage parameters of hamburgers with different fat content cooked until the final core temperature was 71 °C with 3 flips. Data are expressed as means ± standard deviations. Values followed by different letters within the same row indicate significant difference ($p < 0.05$) between samples.

Parameters		B3	A3	A14	A24
Moisture loss (%)	Experimental	17.44 ± 1.21a	18.58 ± 0.96ab	20.03 ± 1.49b	20.79 ± 1.47b
	Computational	21.07	19.97	20.61	20.82
Cooking loss (%)	Experimental	19.17 ± 1.13a	20.71 ± 1.24ab	22.82 ± 1.68b	28.02 ± 1.33c
	Computational	21.67	20.69	24.12	30.24
Fat loss(%)	Exp. by compositional analyses	0.45 ± 1.12a	0.31 ± 0.52a	4.77 ± 0.99b	9.34 ± 1.41c
	Exp. by balance	3.14 ± 0.87a	2.30 ± 1.16a	4.20 ± 0.80b	8.50 ± 0.45c
	Computational	0.60	0.72	3.51	9.42
Moisture loss/initial moisture (%)	Lower region	−13.09 ± 1.36a	−18.19 ± 2.99b	−28.26 ± 2.40c	−34.72 ± 2.30d
	Central region	−5.34 ± 0.78a	−5.09 ± 1.81a	−14.20 ± 2.48b	−16.13 ± 1.57b
	Upper region	−12.94 ± 1.75a	−19.11 ± 2.21b	−32.26 ± 3.38c	−39.65 ± 1.81d
Volume shrinkage (%)	Experimental	24.80 ± 0.37a	25.22 ± 0.46a	26.83 ± 0.87b	28.10 ± 0.56b
	Computational	22.99	24.18	26.81	32.15
Surface shrinkage (%)	Experimental	26.98 ± 2.51a	27.34 ± 1.58ab	29.72 ± 0.86ab	32.50 ± 2.57b
	Computational	23.46	24.63	26.98	32.13

Table 5
Texture parameters of hamburgers with different fat content cooked until the final core temperature was 71 °C with 3 flips. Data are expressed as means ± standard deviations. Values followed by different letters within the same row indicate significant difference ($p < 0.05$) between samples.

Parameters	B3	A3	A14	A24
Hardness (N)	108.43 ± 7.72a	103.88 ± 11.84a	51.18 ± 10.53b	50.72 ± 10.56b
Springiness	0.68 ± 0.03a	0.67 ± 0.02a	0.68 ± 0.02a	0.68 ± 0.02a
Cohesiveness	0.61 ± 0.02a	0.61 ± 0.02a	0.54 ± 0.02b	0.55 ± 0.02b
Gumminess (N)	68.14 ± 8.16a	63.56 ± 6.74a	25.54 ± 6.17b	26.50 ± 3.96b
Chewiness (N)	46.63 ± 5.64a	42.83 ± 5.56a	18.91 ± 6.04b	18.07 ± 2.48b
Maximum shear force (N)	29.27 ± 11.02ab	35.85 ± 7.99a	22.58 ± 3.60b	21.28 ± 7.07b
Work of shearing (N s)	436.86 ± 129.17a	498.70 ± 38.09a	346.19 ± 25.20b	276.22 ± 78.93b
First peak (N)	14.22 ± 4.58a	16.50 ± 3.93a	11.64 ± 3.13ab	7.67 ± 3.93b

opposite: increasing fat levels in ground beef patties yields higher juiciness and tenderness scores despite greater cooking losses (Wong and Maga, 1995; Serdaroglu, 2006; Slayven and Matthews, 2024). This aligns with recent evidence that juiciness perception is driven more by the release of expressed fluid (serum) during mastication than by overall moisture retention (Zhang et al., 2024). It is important to note that extrapolating these findings to other cases should be approached with caution, as grinder plate size and hamburger-forming techniques can significantly influence the perceived texture of patties (Mabrouki et al., 2024).

6. Additional application of the computational model. Predicting fat loss

To assess the network' s performance, before the training, comparisons were made between every split of the raw data and the data that were measured in the experiments. This ensures that the division into different groups is uniform and allows us to determine whether the neural network will be able to correctly predict the output for real hamburgers in the future.

The chosen architecture consists of three fully connected layers: an input layer with 2 neurons, followed by two hidden layers with 4 and 8 neurons respectively, and a final output layer with a single neuron (see Fig. 11). To introduce non-linearity and enhance the model's learning capacity, the Rectified Linear Unit (ReLU) activation function was applied after each layer.

Prior to training, all input features were normalized to the range [0, 1] to ensure stable convergence. The dataset, 1937 valid cookings, was split into training and testing sets (80% and 20%), with a further split of the training set to create a validation subset (20%). Every dataset is shown in Fig. 11. A 5-fold cross-validation was conducted to evaluate the robustness and generalization of the model. Fig. 12 presents the training and validation loss curves, as well as the real vs. predicted values for each fold. Additionally, Table 6 summarizes the MSE, MAE, and R^2 metrics for all folds, including the performance of the global (final) network, demonstrating the consistency of the model across folds. Fig. 12 shows the training history for the five folds, indicating the evolution of the loss (MAE and MSE) during training and validation.

The network was trained using the Adam optimizer, with Mean Average Error (MAE) as the loss function; Mean Squared Error (MSE) was also measured (see Fig. 13). Training was performed over 590 epochs with a batch size of 64; an early stop was included in order not to overfit the neural network.

After training, the test data were evaluated to assess the prediction capability of the network across the entire spectrum for which it was trained. After that, the experimental hamburgers data were also evaluated (see Fig. 14).

7. Conclusions

The findings of this study highlight the value of developing numerical models capable of accurately simulating the complex physical and chemical transformations occurring during meat cooking. Such models can inform practical applications, including the reformulation of meat products to optimize texture and nutritional quality, the design of industrial cooking parameters to improve process efficiency, and the development of consumer guidelines aimed at enhancing food safety and health outcomes. The intrinsic heterogeneity and variability of meat matrices present significant challenges in isolating and quantifying the effects of individual parameters involved in the process, underscoring the need for robust and adaptable modeling approaches.

The model accurately captured experimental trends during domestic pan-cooking of hamburgers with varying fat contents. This predictive capability allowed it to serve as a data generator for training, testing, and validating a neural network designed to estimate fat losses using only the raw hamburger composition. Assessing fat and moisture losses

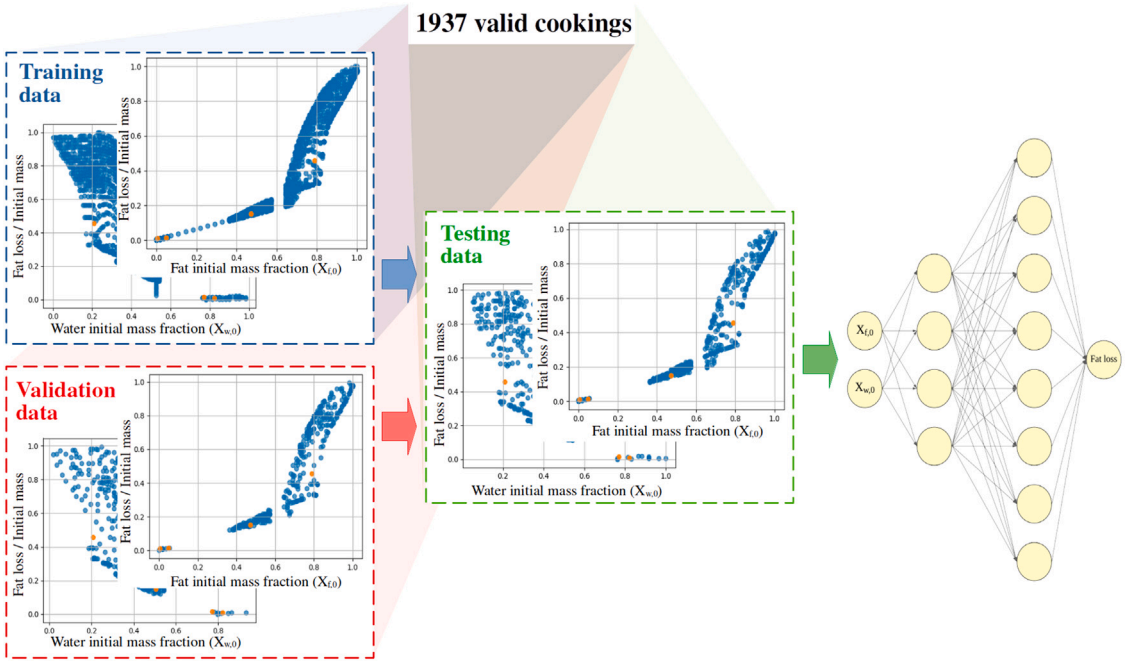

Fig. 11. Schematic representation of the artificial neural network operation. The model receives as input the initial composition data of hamburgers (fat and water mass fractions) and predicts the corresponding fat loss. The dataset of 1937 simulated cooking cases was randomly divided into training (blue), validation (red), and test (green) subsets, as shown in the scatter plots, which display the distribution of input data. Experimental data (orange) were used only for independent testing of the model.

Table 6
Cross-validation results for the five folds and the global (final) network.

Dataset	MSE	MAE	R^2
Fold 1	0.00016	0.00761	0.932
Fold 2	0.00005	0.00375	0.980
Fold 3	0.00004	0.00373	0.983
Fold 4	0.00001	0.00127	0.997
Fold 5	0.00005	0.00409	0.973
Mean ± SD (5 folds)	0.00006 ± 0.00005	0.00409 ± 0.00203	0.973 ± 0.022
Global (final) network	0.00004	0.00374	0.949

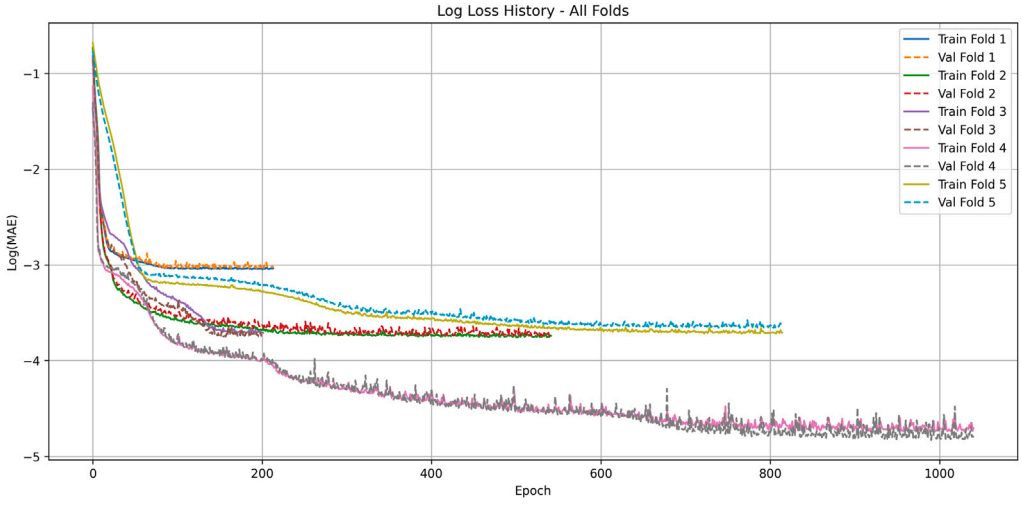

Fig. 12. Training history showing the evolution of MAE for training and validation datasets across the five cross-validation folds. The *x*-axis represents the number of epochs, and the *y*-axis shows the logarithmic error.

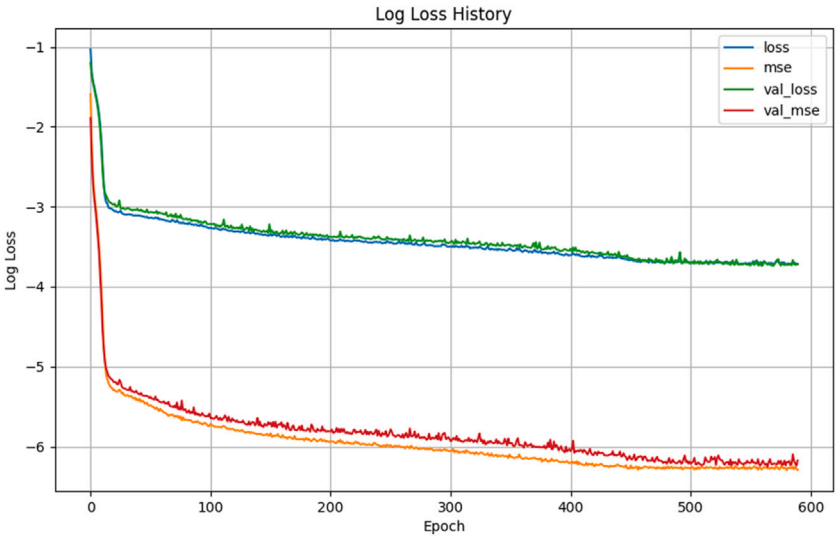

Fig. 13. Training history showing the evolution of MSE and MAE for the training (blue and orange lines) and validation (green and red lines) datasets throughout the epochs. The *x*-axis represents the number of epochs, and the *y*-axis shows the logarithmic error.

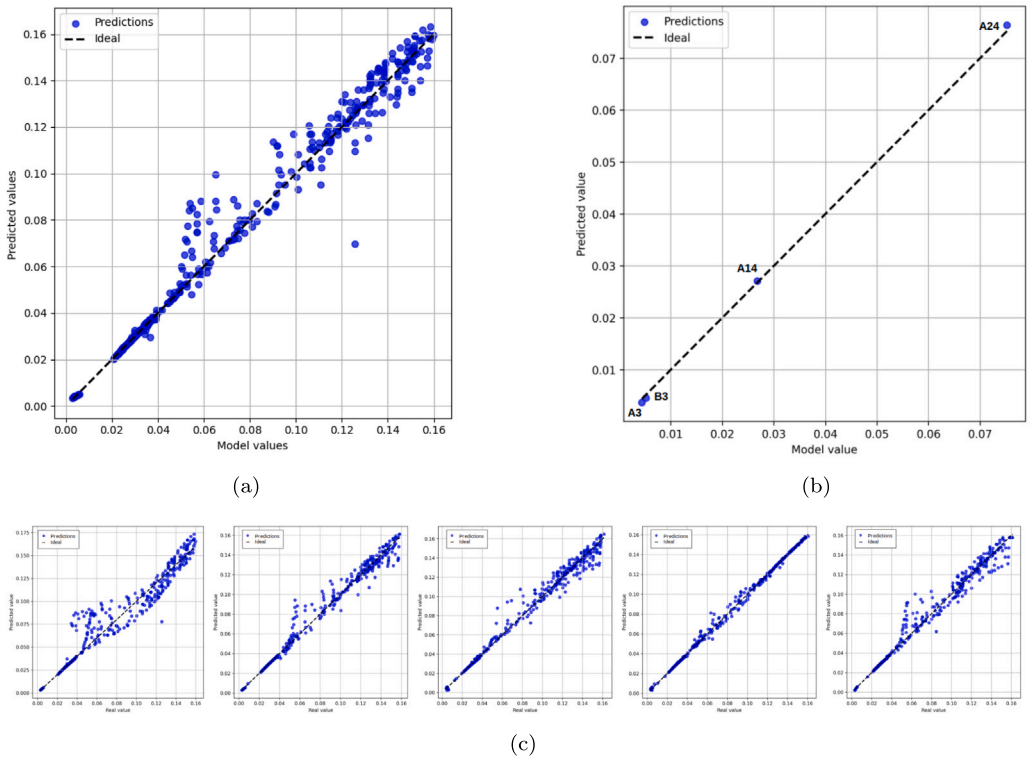

Fig. 14. (a) Model data of fat losses versus predicted data of fat losses for all the spectrum (1937 samples). The ideal agreement is indicated by the diagonal line. (b) Model data of fat losses versus predicted data of fat losses for the burgers analyzed across this study. The ideal agreement is indicated by the diagonal line. (c) Model data versus predicted data for the different folds made (from 1 to 5). The ideal agreement is indicated by the diagonal line.

during cooking is nutritionally relevant, as the initial compositional percentages do not accurately reflect the actual intake by the final consumer. In this context, the neural network emerges as a valuable tool for predicting post-cooking fat content and improving nutritional assessments.

Furthermore, the increasing interest in incorporating fat replacers in hamburger formulations to improve nutritional quality and consumer appeal underscores the relevance of such modeling approaches. Numerical tools capable of predicting the effects of alternative formulations on cooking losses (both water and fat) and on product shrinkage can play a key role in the design and optimization of healthier meat products.

CRediT authorship contribution statement

E. Hernández-Alhambra: Conceptualization, Methodology, Software, Investigation, Writing – original draft. **P. Guiu:** Investigation, Formal analysis, Writing – review & editing. **A. Ferrer-Mairal:** Investigation, Writing – review & editing. **M.A. Martínez:** Investigation, Writing – review & editing. **B. Calvo:** Investigation, Conceptualization,

Methodology, Writing – review & editing, Supervision, Funding acquisition. **J. Grasa:** Investigation, Conceptualization, Writing – review & editing, Funding acquisition. **M.L. Salvador:** Investigation, Conceptualization, Methodology, Writing – original draft, Writing – review & editing, Supervision, Funding acquisition.

Declaration of competing interest

The authors declare the following financial interests/personal relationships which may be considered as potential competing interests: Jorge Grasa reports financial support was provided by Spain Ministry of Science and Innovation. Maria Luisa Salvador reports financial support was provided by European Union. Begona Calvo reports financial support was provided by Government of Aragon Department of Science Technology and University. Begona Calvo reports a relationship with BSH Home Appliances Group that includes: funding grants. If there are other authors, they declare that they have no known competing financial interests or personal relationships that could have appeared to influence the work reported in this paper.

Acknowledgments

This work was supported by project CPP2021-008938 HIPATIA financed by the Spanish Ministry of Science and Innovation MCIN/AEI/ 10.13039/ 501100011033 and by the European Union "NextGenerationEU/PRTR"; and by the BSH Home Appliances Group. It has also been supported by the Department of Industry and Innovation (Government of Aragon) through the research group Grant T24-23R and T07-23R. Additional support was provided by the Government of Aragón under grant number PROY-T03-24 IACOOK. Authors acknowledge the use of instrumentation as well as the technical advice provided by the National Facility ELECMI ICTS node "Laboratorio de Microscopías Avanzadas" at the University of Zaragoza.

References

Ahmad, S., Khan, M.A., Kamil, M., 2015. Mathematical modeling of meat cylinder cooking. LWT - Food Sci. Technol. 60, 678–683. http://dx.doi.org/10.1016/j.lwt.2014.10.061.

AOAC International, 2002. Official method 950.46. Moisture in meat. In: Official Methods of Analysis of AOAC International, sixteenth ed. AOAC International, Gaithersburg, MD.

Badar, I.H., Wang, Z., Zhou, Y., Guo, X., Jaspal, M.H., Kong, B., Liu, H., 2024. Effect of flaxseed-derived diglyceride-based high internal phase pickering emulsion on the quality characteristics of reformulated beef burgers. Meat Sci. 212, 109474. http://dx.doi.org/10.1016/j.meatsci.2024.109474.

Barbera, S., Tassone, S., 2006. Meat cooking shrinkage: Measurement of a new meat quality parameter. Meat Sci. 73, 467–474. http://dx.doi.org/10.1016/j.meatsci.2006.01.011.

Bastos, S.C., Pimenta, M.E.S.G., Pimenta, C.J., Reis, T.A., Nunes, C.A., Pinheiro, A.C.M., Fabrício, L.F.F., Leal, R.S., 2014. Alternative fat substitutes for beef burger: technological and sensory characteristics. J. Food Sci. Technol. 51, 2046–2053. http://dx.doi.org/10.1007/s13197-013-1233-2.

Berger, L.M., Witte, F., Tomasevic, I., Heinz, V., Weiss, J., Gibis, M., Terjung, N., 2023. A review on the relation between grinding process and quality of ground meat. Meat Sci. 205, 109320. http://dx.doi.org/10.1016/j.meatsci.2023.109320.

Brewer, M.S., 2012. Reducing the fat content in ground beef without sacrificing quality: A review. Meat Sci. 91, 385–395. http://dx.doi.org/10.1016/j.meatsci.2012.02.024.

Chapwanya, M., Misra, N., 2015. A mathematical model of meat cooking based on polymer-solvent analogy. Appl. Math. Model. 39, 4033–4043. http://dx.doi.org/10.1016/j.apm.2014.12.015.

Choi, Y., Okos, M.R., 1986. Effects of temperature and composition on thermal properties of foods. J. Food Process. Appl. 1, 93–101.

Dalvi-Isfahan, M., 2023. Mathematical modeling for investigating the effect of single-sided flipping on moisture, fat content, and safety of hamburger patty. J. Food Process. Eng. 46, e14450. http://dx.doi.org/10.1111/jfpe.14450.

de Albuquerque, C.D., Curet, S., Boillereaux, L., 2019. A 3d-cfd-heat-transfer-based model for the microbial inactivation of pasteurized food products. Innov. Food Sci. Emerg. Technol. 54, 172–181. http://dx.doi.org/10.1016/j.ifset.2019.04.007.

Dhall, A., Datta, A.K., 2011. Transport in deformable food materials: A poromechanics approach. Chem. Eng. Sci. 66, 6482–6497. http://dx.doi.org/10.1016/j.ces.2011.09.001.

Dhall, A., Halder, A., Datta, A.K., 2012. Multiphase and multicomponent transport with phase change during meat cooking. J. Food Eng. 113, 299–309. http://dx.doi.org/10.1016/j.jfoodeng.2012.05.030.

Duconseille, A., Astruc, T., Sasaki, K., Motoyama, M., 2022. Transformation of highly marbled meats under various cooking processes. Meat Sci. 189, 108810. http://dx.doi.org/10.1016/j.meatsci.2022.108810.

Feyissa, A.H., Gernaey, K.V., Adler-Nissen, J., 2013. 3d modelling of coupled mass and heat transfer of a convection-oven roasting process. Meat Sci. 93, 810–820. http://dx.doi.org/10.1016/j.meatsci.2012.12.003.

Goñi, S.M., Salvadori, V.O., 2010. Prediction of cooking times and weight losses during meat roasting. J. Food Eng. 100, 1–11. http://dx.doi.org/10.1016/j.jfoodeng.2010.03.016.

Hernández-Alhambra, E., Guíu, P., Cabeza-Gil, I., Ferrer-Mairal, A., Martínez, M.A., Calvo, B., Grasa, J., Salvador, M.L., 2024. Towards domestic cooking efficiency: A case study on burger pan frying using experimental and computational results. J. Food Eng. 363, 111783. http://dx.doi.org/10.1016/j.jfoodeng.2023.111783.

Hernández-Alhambra, E., Guíu, P., Ferrer-Mairal, A., Martínez, M.A., Calvo, B., Grasa, J., Salvador, M.L., 2025. Predicting optimal flipping conditions during burger pan cooking with a numerical model. J. Food Eng. 387, 112315. http://dx.doi.org/10.1016/j.jfoodeng.2024.112315.

ISO, 1973. Official Method 1443: Meat and Meat Products-Determination of Total Fat Content. International Organization for Standardization.

ISO, 2008. Official Method 16634-1: Food Products - Determination of the Total Nitrogen Content by Combustion According to the Dumas Principle and Calculation of the Crude Protein Content. International Organization for Standardization.

ISO, 2023. Official Method 1442: Meat and Meat Products-Determination of Moisture Content-Reference Method, third ed. International Organization for Standardization.

Kirkyol, M., Akköse, A., 2023. Effects of animal fat replacement with almond flour on quality parameters of beef patties. Food Sci. Nutr. 11, 7091–7099. http://dx.doi.org/10.1002/fsn3.3633.

Liu, Y., Liu, C., Huang, X., Li, M., Zhao, G., Sun, L., Yu, J., Deng, W., 2024. Exploring the role of maillard reaction and lipid oxidation in the advanced glycation end products of batter-coated meat products during frying. Food Res. Int. 178, 113901. http://dx.doi.org/10.1016/j.foodres.2023.113901.

Liu, W., Luo, X., Huang, Y., Zhao, M., Liu, T., Wang, J., Feng, F., 2023. Influence of cooking techniques on food quality, digestibility, and health risks regarding lipid oxidation. Food Res. Int. 167, 112685. http://dx.doi.org/10.1016/j.foodres.2023.112685.

Lucherk, L.W., O'Quinn, T.G., Legako, J.F., Rathmann, R.J., Brooks, J.C., Miller, M.F., 2017. Assessment of objective measures of beef steak juiciness and their relationships to sensory panel juiciness ratings1,2. J. Anim. Sci. 95, 2421–2437. http://dx.doi.org/10.2527/jas.2016.0930.

Mabrouki, S., Abid, K., Kaihara, H., Patrucco, S.G., Tassone, S., Barbera, S., 2024. Assessing texture profile analysis in natural state versus texture profile analysis with back extrusion post-homogenization of cooked pea protein-based and meat patties: A comparative study. Futur. Foods 9, 100345. http://dx.doi.org/10.1016/j.fufo.2024.100345.

Mathijssen, A.J.T.M., Lisicki, M., Prakash, V.N., Mossige, E.J.L., 2023. Culinary fluid mechanics and other currents in food science. Rev. Modern Phys. 95, 025004. http://dx.doi.org/10.1103/RevModPhys.95.025004.

Moya, J., Lorente-Bailo, S., Ferrer-Mairal, A., Martínez, M.A., Calvo, B., Grasa, J., Salvador, M.L., 2021a. Color changes in beef meat during pan cooking: kinetics, modeling and application to predict turn over time. Eur. Food Res. Technol. 247, 2751–2764. http://dx.doi.org/10.1007/s00217-021-03821-y.

Moya, J., Lorente-Bailo, S., Salvador, M.L., Ferrer-Mairal, A., Martínez, M.A., Calvo, B., Grasa, J., 2021b. Development and validation of a computational model for steak double-sided pan cooking. J. Food Eng. 298, 110498. http://dx.doi.org/10.1016/j.jfoodeng.2021.110498.

Nelson, H., Deyo, S., Granzier-Nakajima, S., Puente, P., Tully, K., Webb, J., 2020. A mathematical model for meat cooking. Eur. Phys. J. Plus 135, http://dx.doi.org/10.1140/epjp/s13360-020-00311-0.

Niu, L., Rasco, B.A., Tang, J., Lai, K., Huang, Y., 2015. Relationship of changes in quality attributes and protein solubility of ground beef under pasteurization conditions. LWT - Food Sci. Technol. 61, 19–24. http://dx.doi.org/10.1016/j.lwt.2014.11.016.

Onopiuk, A., Kolodziejczak, K., Szpicer, A., Wojtasik-Kalinowska, I., Wierzbicka, A., Półtorak, A., 2021. Analysis of factors that influence the pah profile and amount in meat products subjected to thermal processing. Trends Food Sci. Technol. 115, 366–379. http://dx.doi.org/10.1016/j.tifs.2021.06.043.

Oroszvári, B.K., Bayod, E., Sjöholm, I., Tornberg, E., 2006a. The mechanisms controlling heat and mass transfer on frying of beefburgers. III. Mass transfer evolution during frying. J. Food Eng. 76, 169–178. http://dx.doi.org/10.1016/j.jfoodeng.2005.05.018.

Oroszvári, B.K., Sofia Rocha, C., Sjoholm, I., Tornberg, E., 2006b. Permeability and mass transfer as a function of the cooking temperature during the frying of beefburgers. J. Food Eng. 74, 1–12. http://dx.doi.org/10.1016/j.jfoodeng.2005.02.024.

Otto, J.R., Mwangi, F.W., Pewan, S.B., Adegboye, O.A., Malau-Aduli, A.E.O., 2022. Lipogenic gene single nucleotide polymorphic dna markers associated with intramuscular fat, fat melting point, and health-beneficial omega-3 long-chain polyunsaturated fatty acids in australian pasture-based bowen genetics forest pastoral angus, hereford, and wagyu beef cattle. Genes 13, 1411. http://dx.doi.org/10.3390/genes13081411.

Ou, D., Mittal, G., 2007. Single-sided pan frying of frozen hamburgers with flippings for microbial safety using modeling and simulation. J. Food Eng. 80, 33–45. http://dx.doi.org/10.1016/j.jfoodeng.2006.03.033.

Pan, Z., Singh, R.P., 2001. Physical and thermal properties of ground beef during cooking. LWT - Food Sci. Technol. 34, 437–444. http://dx.doi.org/10.1006/fstl.2001.0762.

Pan, Z., Singh, R., Rumsey, T., 2000. Predictive modeling of contact-heating process for cooking a hamburger patty. J. Food Eng. 46, 9–19. http://dx.doi.org/10.1016/S0260-8774(00)00063-7.

Roldan, M., Antequera, T., Armenteros, M., Ruiz, J., 2014. Effect of different temperature-time combinations on lipid and protein oxidation of sous-vide cooked lamb loins. Food Chem. 149, 129–136. http://dx.doi.org/10.1016/j.foodchem.2013.10.079.

Serdaroglu, M., 2006. The characteristics of beef patties containing different levels of fat and oat flour. Int. J. Food Sci. Technol. 41, 147–153. http://dx.doi.org/10.1111/j.1365-2621.2005.01041.x.

Sheen, S., Huang, L., Hwang, C.A., 2024. Numerical simulation of heat transfer during meat ball cooking and microbial food safety enhancement. J. Food Sci. 89, 1632–1641. http://dx.doi.org/10.1111/1750-3841.16949.

Sheridan, P.S., Shilton, N.C., 2002. Determination of the thermal diffusivity of ground beef patties under infrared radiation oven-shelf cooking. J. Food Eng. 52, 39–45. http://dx.doi.org/10.1016/S0260-8774(01)00083-8.

Shi, Y., Li, J., Zhou, L., Zhang, J., Feng, X., Xing, W., Tang, C., Bai, Y., 2025. Exploring the contribution of phosphatidylcholine and triglyceride on the formation of beef aroma-active compounds with thermal oxidation system. Curr. Res. Food Sci. 10, 100973. http://dx.doi.org/10.1016/j.crfs.2025.100973.

Shilton, N., Mallikarjunan, P., Sheridan, P., 2002. Modeling of heat transfer and evaporative mass losses during the cooking of beef patties using far-infrared radiation. J. Food Eng. 55, 217–222. http://dx.doi.org/10.1016/s0260-8774(02)00066-3.

Slayven, S., Matthews, K., 2024. Meat and Reformed Meat Products. Springer International Publishing, Cham, http://dx.doi.org/10.1007/978-3-031-41900-3_15.

Sobral, M.M.C., Casal, S., Faria, M.A., Cunha, S.C., Ferreira, I.M.L.O., 2020. Influence of culinary practices on protein and lipid oxidation of chicken meat burgers during cooking and in vitro gastrointestinal digestion. Food Chem. Toxicol. 141, 111401. http://dx.doi.org/10.1016/j.fct.2020.111401.

Souppez, J.B.R.G., Dages, B.A.S., Pavar, G.S., Thomas, J.M., Fabian, J., Theodosiou, E., 2025. Mechanical properties and texture profile analysis of beef burgers and plant-based analogues. J. Food Eng. 385, 112259. http://dx.doi.org/10.1016/j.jfoodeng.2024.112259.

Straub, J., 1985. NBS/NRC steam tables. VonL. haar, j. s. gallagher undG. s. kell. hemisphere publishing corp., washington-new york-london 1984. 1. aufl., XII, 320 s., geb., $ 34.50. Chem. Ing. Tech. 57, http://dx.doi.org/10.1002/cite.330570931, 812–812.

Szpicer, A., Wierzbicka, A., Półtorak, A., 2022. Optimization of beef heat treatment using cfd simulation: Modeling of protein denaturation degree. J. Food Process. Eng. 45, e14014. http://dx.doi.org/10.1111/jfpe.14014.

Tornberg, E., 2005. Effects of heat on meat proteins - implications on structure and quality of meat products. Meat Sci. 70, 493–508. http://dx.doi.org/10.1016/j.meatsci.2004.11.021.

Tornberg, E., 2013. Engineering processes in meat products and how they influence their biophysical properties. Meat Sci. 95, 871–878. http://dx.doi.org/10.1016/j.meatsci.2013.04.053.

van der Sman, R., 2007. Moisture transport during cooking of meat: An analysis based on Flory–Rehner theory. Meat Sci. 76, 730–738. http://dx.doi.org/10.1016/j.meatsci.2007.02.014.

Vaskoska, R., Ha, M., Ong, L., Chen, G., White, J., Gras, S., Warner, R., 2021. Myosin sensitivity to thermal denaturation explains differences in water loss and shrinkage during cooking in muscles of distinct fibre types. Meat Sci. 179, 108521. http://dx.doi.org/10.1016/j.meatsci.2021.108521.

Vu, G., Zhou, H., McClements, D.J., 2022. Impact of cooking method on properties of beef and plant-based burgers: Appearance, texture, thermal properties, and shrinkage. J. Agric. Food Res. 9, 100355. http://dx.doi.org/10.1016/j.jafr.2022.100355.

Wong, N., Maga, J., 1995. The effect of fat content on the quality of ground beef patties. In: Charalambous, G. (Ed.), Food Flavors: Generation, Analysis and Process Influence. In: Developments in Food Science, vol. 37, Elsevier, pp. 1345–1351. http://dx.doi.org/10.1016/S0167-4501(06)80237-2.

Xia, C., Wen, P., Yuan, Y., Yu, X., Chen, Y., Xu, H., Cui, G., Wang, J., 2021. Effect of roasting temperature on lipid and protein oxidation and amino acid residue side chain modification of beef patties. RSC Adv. 11, 21629–21641. http://dx.doi.org/10.1039/D1RA03151A.

Yan, Z., Sousa-Gallagher, M.J., Oliveira, F.A., 2008. Shrinkage and porosity of banana, pineapple and mango slices during air-drying. J. Food Eng. 84, 430–440. http://dx.doi.org/10.1016/j.jfoodeng.2007.06.004.

Zhang, Y., Brouwer, R., Sala, G., Scholten, E., Stieger, M., 2024. Exploring relationships between juiciness perception, food and bolus properties of plant-based meat analogue and beef patties. Food Hydrocolloids 147, 109443. http://dx.doi.org/10.1016/j.foodhyd.2023.109443.

Zorrilla, S.E., Singh, R., 2003. Heat transfer in double-sided cooking of meat patties considering two-dimensional geometry and radial shrinkage. J. Food Eng. 57, 57–65. http://dx.doi.org/10.1016/S0260-8774(02)00273-X.